Magnetic phase diagram of the two-dimensional Heisenberg spin one-half canted antiferromagnet ethyl-ammonium tetrabromocuprate(II)

by Yadollah Hassani

A thesis submitted in partial fulfillment of the requirements for the degree of Master of Science in Physics

Montana State University

Abstract:
The magnetic susceptibility of (C2H5NH3)2CuBr4 has been studied as a function of an applied field (0-5500 Oe) and of temperature (1.85-120 K). The data show the antiferromagnetic ordering along b to occur at Tc =10.78 K, but the moments are canted toward the c-axis. The data in the paramagnetic region is fitted to the simple quadratic Heisenberg model. From this fit values for the exchange energy J/k = 18.5 K, Curie constant, C = .45 emu-K/mole, Curie-Weiss temperature,6 =37 K and J/kT. = 1.72 have been obtained. The anisotropic exchange field, Hd =2600 t)e, the inter-layer exchange field, Haf =300 Ge and out of layer anisotropy field, Ha =1550 Ge are obtained by means of mean field calculation. The magnetic phase diagrams have been constructed along a, b, and c axes by means of susceptibility versus temperature and magnetization curves. We find the bieritical point at 10.74 K and 60 tie, spin twist field, Hst =80 Oe, and derive the angle between the c- axis and the moment direction to be 53.2 degrees.

MAGNETIC PHASE DIAGRAM OF THE TWO-DIMENSIONAL HEISENBERG SPIN ONE-HALF CANTED ANTIFERROMAGNET ETHYL-AMMONIUM TETRABROMOCUPRATE(II)

by

Yadollah Hassani

A thesis submitted in partial fulfillment
of the requirements for the degree

of

Master of Science

in

Physics

MONTANA STATE UNIVERSITY
Bozeman, Montana

November 1988

APPROVAL

of a thesis submitted by

Yadollah Hassani

This thesis has been read by each member of the thesis committee and has been found to be satisfactory regarding content, English usage, format, citations, bibliographic style, and consistency, and is ready for submission to the College of Graduate Studies.

12/1/88
Date

Chairperson, Graduate Committee

Approved for the Major Department

12/1/88
Date

Head, Major Department

Approved for the College of Graduate Studies

12/13/88
Date

Graduate Dean

STATEMENT OF PERMISSION TO USE

In presenting this thesis in partial fulfillment of the requirements for a master's degree at Montana State University, I agree that the Library shall make it available to borrowers under rules of the Library. Brief quotations from this thesis are allowable without special permission, provided that accurate acknowledgment of source is made.

Permission for extensive quotation from or reproduction of this thesis may be granted by my major professor, or in his absence, by the Dean of Libraries when, in the opinion of either, the proposed use of the material is for scholarly purposes. Any copying or use of the material in this thesis for financial gain shall not be allowed without my written permission.

Signature H Hassani

Date 12/1/88

ACKNOWLEDGEMENTS

I would like to express my sincere appreciation to all the people who contributed in making this research possible. My deepest gratitude goes to my advisor, John E. Drumheller, who guided me with continual support and encouragement. I must also acknowledge the efforts of all the others who greatly assisted me, Jerry Rubenacker, George Tuthill, Hugo Schmidt, Stuart Hutton, Donald Haines, Kenneth Emerson, and (Ravi) Ravindran. My special thanks to all the staff, faculty and my friends in the Physics Department, whom I may not have mentioned by name.

Financial support for research provided by NSF grant DMR-8702933.

TABLE OF CONTENTS

LIST OF TABLES

LIST OF FIGURES

LIST OF FIGURES-Continued

LIST OF FIGURES-Continued

LIST OF FIGURES-Continued

ABSTRACT

The magnetic susceptibility of $(C_2H_5NH_3)_2CuBr_4$ has been studied as a function of an applied field (0-5500 Oe) and of temperature (1.85-120 K). The data show the antiferromagnetic ordering along b to occur at T_c =10.78 K, but the moments are canted toward the c-axis. The data in the paramagnetic region is fitted to the simple quadratic Heisenberg model. From this fit values for the exchange energy J/k = 18.5 K, Curie constant, C = .45 emu-K/mole, Curie-Weiss temperature,θ =37 K and J/kT_c = 1.72 have been obtained. The anisotropic exchange field, H_d =2600 Oe, the inter-layer exchange field, H_{AF} =300 Oe and out of layer anisotropy field, H_a =1550 Oe are obtained by means of mean field calculation. The magnetic phase diagrams have been constructed along a, b, and c axes by means of susceptibility versus temperature and magnetization curves. We find the bicritical point at 10.74 K and 60 Oe, spin twist field, H_{ST} =80 Oe, and derive the angle between the c-axis and the moment direction to be 53.2 degrees.

CHAPTER ONE

INTRODUCTION

The purpose of this investigation is to analyze the magnetic properties of $[C_2H_5NH_3]_2CuBr_4$ and construct magnetic phase diagrams along all three axes. $[C_2H_5NH_3]_2CuBr_4$ is a member of the $[C_nH_{2n+1}NH_3]_2CuX_4$ family, hereafter abbreviated as C_nX where X represents a Cl or Br atom and n varies from 1 to 10. C_nX compounds have attracted special attention because they can serve as an approximation to the ideal two dimensional spin 1/2 Heisenberg ferromagnets. In the two dimensional Heisenberg S = 1/2 ideal system, exchange interactions are confined to two dimensions, and long range order above zero K cannot be sustained. However, C_nX compounds order at a temperature $[T_c]$ between 7 K to 16 K. This series of compounds deviate from the ideal system due to the presence of a weak anisotropy and coupling in the third dimension, which in turn causes the long range ordering at a temperature higher than zero K.

Yoshio reported this compound to be a weak ferromagnet. Weak ferromagnetism occurs mainly in antiferromagnetic crystals such as α-Fe_20_3, NiF_2, $MnCO_3$, and $CoCO_3$. The problem of weak ferromagnetism was first studied by Dzialoshinski [2] who contributed the weak ferromagnetism to an interaction of the form $d\circ[S_1XS_2]$. This term represents the antisymmetric part of the spin coupling. In contrast Yoshio claims that the source of the canting is symmetrical, i.e., of the

form $S_1 \circ K_s \circ S_2$. This discrepancy prompted us to do further investigation on this compound. Also, we have confusing ac susceptibility data.

Although the crystal structure of C_nX compounds are similar, the magnetic behaviors of the members of this family differ from one another. For instance, the ferromagnetic layers may couple antiferromagnetically as in C_2Cl [1]. In C_1Cl, the coupling between layers is ferromagnetic [1]. On the other hand, in C_3Br a weak ferromagnetic moment appears along the c-axis [1]. The ferromagnetic intra-layer exchange constant, J/k, varies from 15.4 K for C_4Cl to 22 K for C_5Br [3]. Inter-layer interaction, J'/k, is very weak compared to that of in-plane interaction, $J'/J=1.7\times10^{-3}$ for C_1Br and $J'/J=10^{-5}$ for $C_{10}Cl$ [4]. For C_2Br, different values of J'/J have been reported. Yoshio reports $Z'|J'|/ZJ=7\times10^{-4}$ where Z is the number of nearest neighbors in the plane and Z' is the number of nearest neighbors in the next plane. If we take Z=4 and $Z'=8$ then we get $J'/J=3.5\times10^{-4}$. L. de Jongh gives a value of 1.7×10^{-3} which is about 4.8 times larger than Yoshio's J'/J value. Although inter-layer exchange coupling is small, it plays a major role in the magnetic behavior of C_nX compounds below the transition temperature. The anisotropy field within the layer is of the order of 10^{-5} to 10^{-4} of the ferromagnetic exchange field. The out-of-plane anisotropy remains the same for all compounds and is of order of 10^{-3} of the ferromagnetic exchange field [4].

The crystal structure of the known members of the C_nX family is orthorhombic [4], which means the axes of a unit cell are perpendicular and also $a\neq b\neq c$. In this series of compounds a and b are nearly equal,

but the distance between the planes increases as n is increased. Table I is taken from reference [5] where d_1 is the distance between copper ions within a layer and d_2 is the distance between nearest neighbor copper ions in different layers. It also shows lattice constants up to n=6. For C_2Br a transition of 10.72 K is given. We measured the transition temperature to be 10.75 ± 0.05 K . Professor K. E. Emerson, of Montana State University, has measured the lattice constants of C_2Br to be a=7.9525, b=7.7187, and c=21.4191 Angstrom which is in agreement with Table 1.

The second chapter of this thesis is concerned with the theoretical behavior of antiferromagnets. Chapter Three deals with methodology, and includes a discussion of susceptibility versus temperature and field. In Chapter Four, mean field calculations are carried out and numerical values for magnetic parameters are given. Finally, in Chapter Five, magnetic phase diagrams along three axis are constructed and discussed.

Table 1: Curie temperature and lattice constants

Compound	T_c(K)	a_o(Å)	b_o(Å)	c_o(Å)	d_1(Å)	d_2(Å)
C_1Cl	8.9	7.54	7.3	18.55	5.24	9.99
C_2Cl	10.2	7.47	7.35	21.18	5.24	11.22
C_3Cl	7.61	7.65	7.33	24.66	5.29	12.89
C_4Cl	7.27					
C_5Cl	7.25	7.51	7.38	34.81	5.26	17.8
C_6Cl	7.65					
C_2Br	10.72	7.95	7.72	21.5	5.54	11.44
C_3Br	10.41	8.00	7.69	24.32	5.54	12.78

CHAPTER TWO

THEORETICAL BEHAVIOR OF ANTIFERROMAGNETS

Susceptibility as a Function of Temperature

An antiferromagnet consists of two or more magnetic sublattices. The simplest antiferromagnetic arrangement is one in which the magnetic atoms can be subdivided into two sublattices, A and B, so that moments belonging to sublattice A point in one direction, and those belonging to sublattice B point in the opposite direction. The magnetic interaction between the sublattices is such that, below the Neel temperature [T_N], spins on the sublattice A point in a positive direction and those of sublattice B point in a negative direction, leading to zero net moment. The direction of the magnetization of each sublattice below the Neel temperature will be along the direction of the anisotropy field. This is called easy direction or easy axis.

Cooling a paramagnet in zero applied field leads to a transition from the paramagnetic to antiferromagnetic state at the Neel temperature. Above the Neel temperature, the system behaves as a paramagnetic system and obeys the Curie-Weiss law:

$$\chi=C/(T-\theta)$$

where C and θ are called Curie constant and Curie temperature, respectively. The susceptibility below the Neel temperature along the

easy axis decreases reaching a finite value at T=0. This is illustrated in Figure 1.

In cooling a paramagnetic system, if a constant external field is applied normal to the easy axis, the applied field will produce a torque that tends to rotate the sublattice magnetization. The internal field will oppose this rotation. One can show, by molecular field calculation, that the susceptibility below the Neel temperature remains constant and assumes a value of C/2 (see Figure 2).

On the other hand, if the external field is applied parallel to the easy axis, the susceptibility decreases below the Neel temperature and goes to zero at T=0, as shown in Figure 2. This is because there is a strong interaction between the moments of the two sublattices and a relatively small applied field cannot turn over the moments of the negative sublattice to the direction of the field (Figure 2).

In a powder sample in which the easy directions are distributed at random, the susceptibility is given by

$$\chi_{pow} = (1/3)\,\chi_{pa} + (2/3)\,\chi_{pe}$$

where χ_{pa} and χ_{pe} denote the parallel and perpendicular susceptibility, respectively, as shown in Figure 2.

Magnetization as a Function of Field

A magnetization curve [M vs H] yields an important feature of a magnetic system, the strength of the anisotropy field. For an antiferromagnet, we can consider two cases: field applied 1] normal to the easy axis and 2] parallel to it.

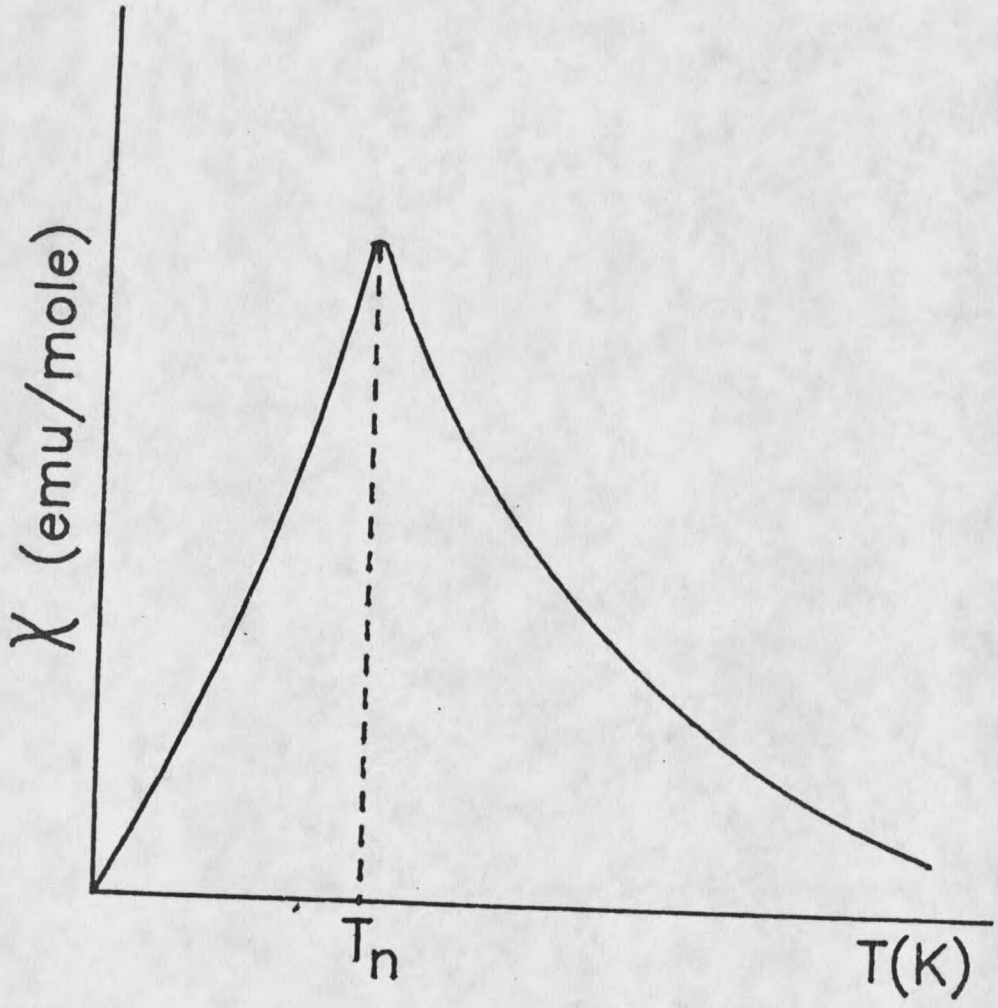

Figure 1. The magnetic susceptibility of an antiferromagnet at zero field

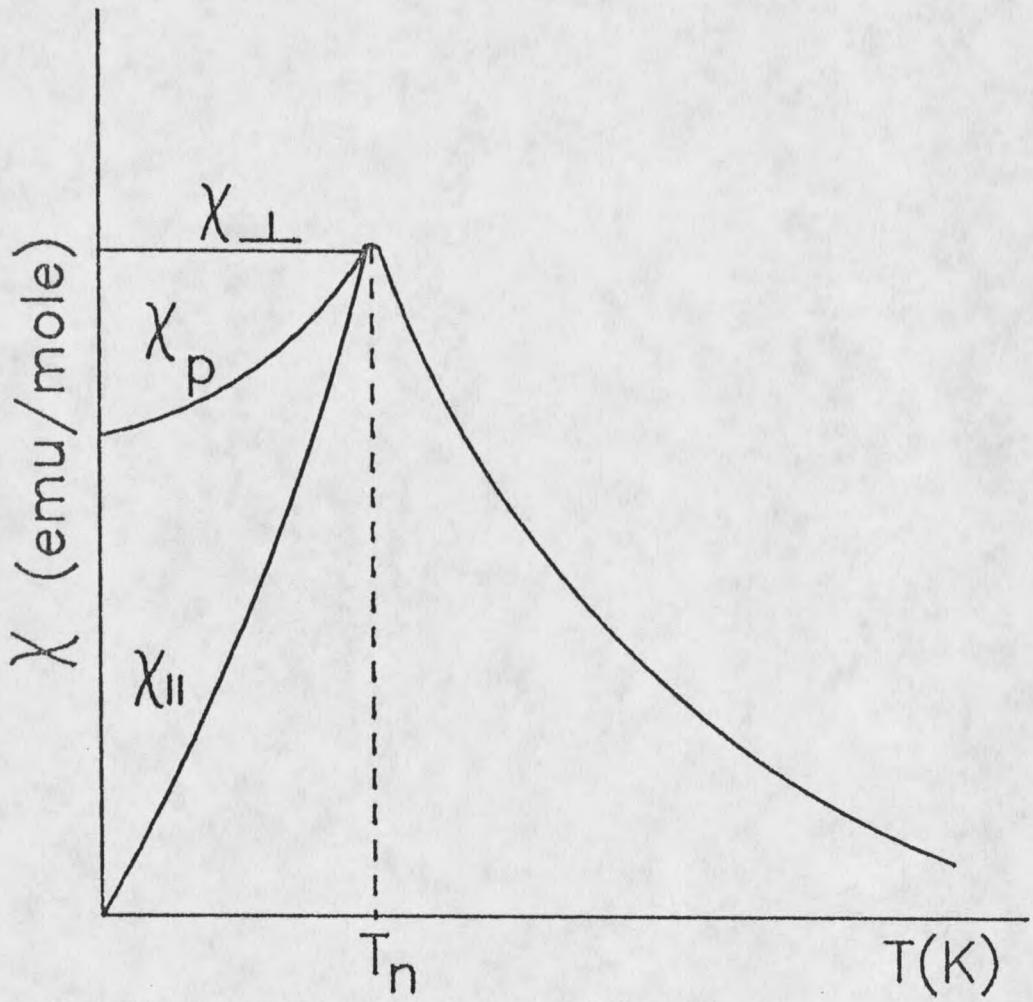

Figure 2. Thermal variation of molar susceptibility of an antiferromagnetic in the presence of relatively weak field

1] Field normal to easy axis: an increasing applied field, H, will turn each sublattice magnetization away from the easy axis and tends to align it in the direction of the applied field. As field is increased, magnetization will increase linearly until saturation is achieved. This gives the magnetization versus field curve shown in Figure 3.

2] Field parallel to easy axis: for a field applied in the direction of the easy axis, the applied field will be resisted by the anisotropy field until the applied field equals that of the anisotropy field. This field is called spin-flop field. At the spin-flop field two sublattice magnetization will reorient themselves such that they are perpendicular to the direction of the applied field. As the field is increased further, magnetization will increase linearly as a function of the applied field until saturation is acheived. This is shown in Figure 4.

We will show that, below some critical temperature, an antiferromagnetic ordering develops in C_2Br. In contrast to the usual antiferromagnets, the magnetization vectors of the sublattices are not exactly antiparallel to each other, but are inclined at some angle. In C_2Br spin-flop does not occur. However, a spin rearrangement occurs, which we will call a spin-twist transition.

Magnetic Phase Diagram

A magnetic phase diagram [H_a vs T] can be constructed for an ordered system to illustrate the phases that occur. A hypothetical phase diagram for an antiferromagnet when small anisotropy with the external field applied parallel to the easy axis is shown in Figure 5.

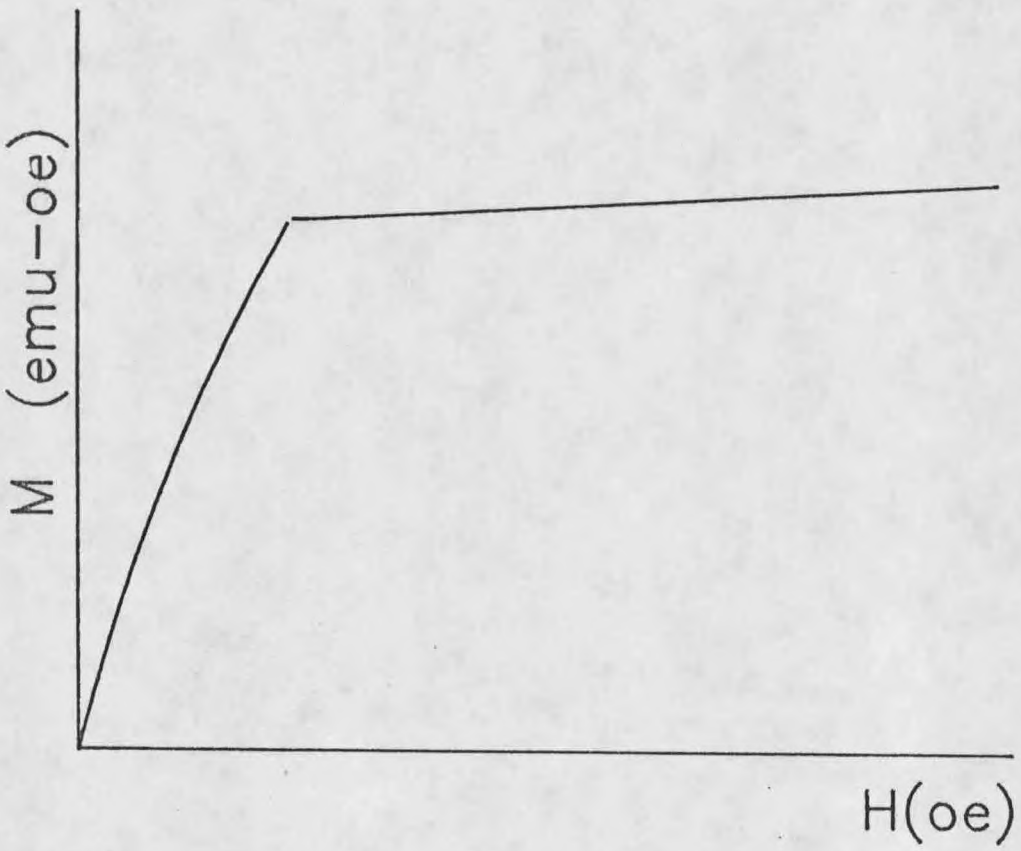

Figure 3. Magnetization versus field. Field is applied perpendicular to the easy axis

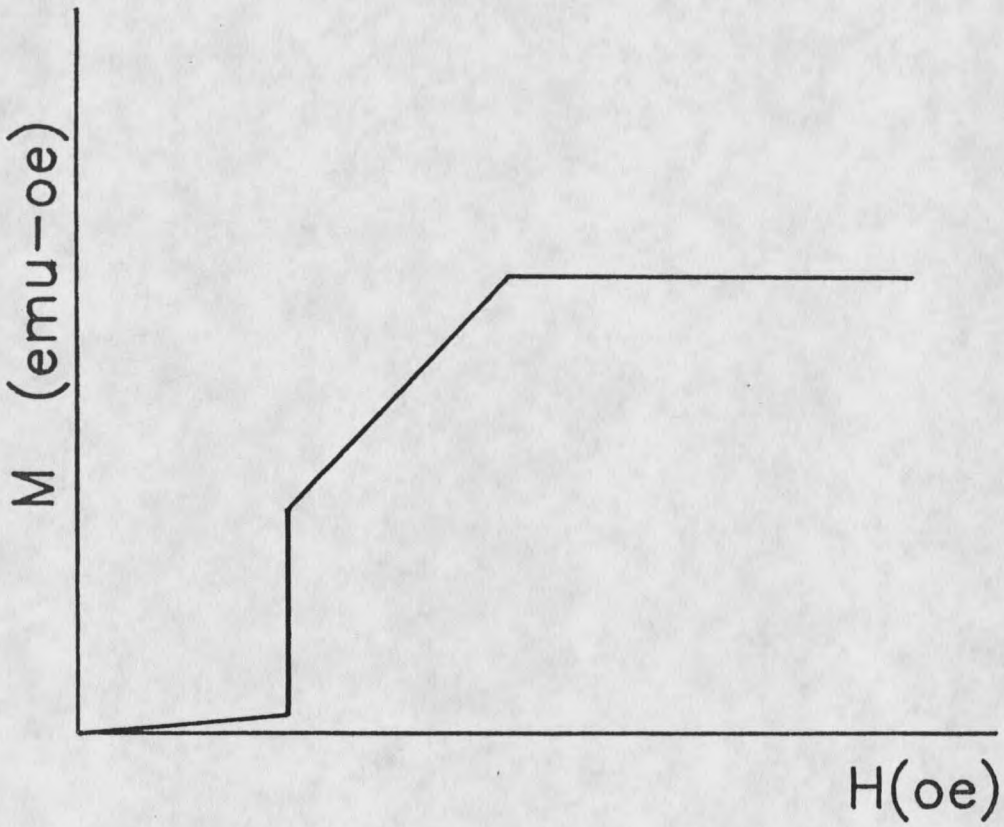

Figure 4. Magnetization versus field. Field is applied parallel to the easy axis

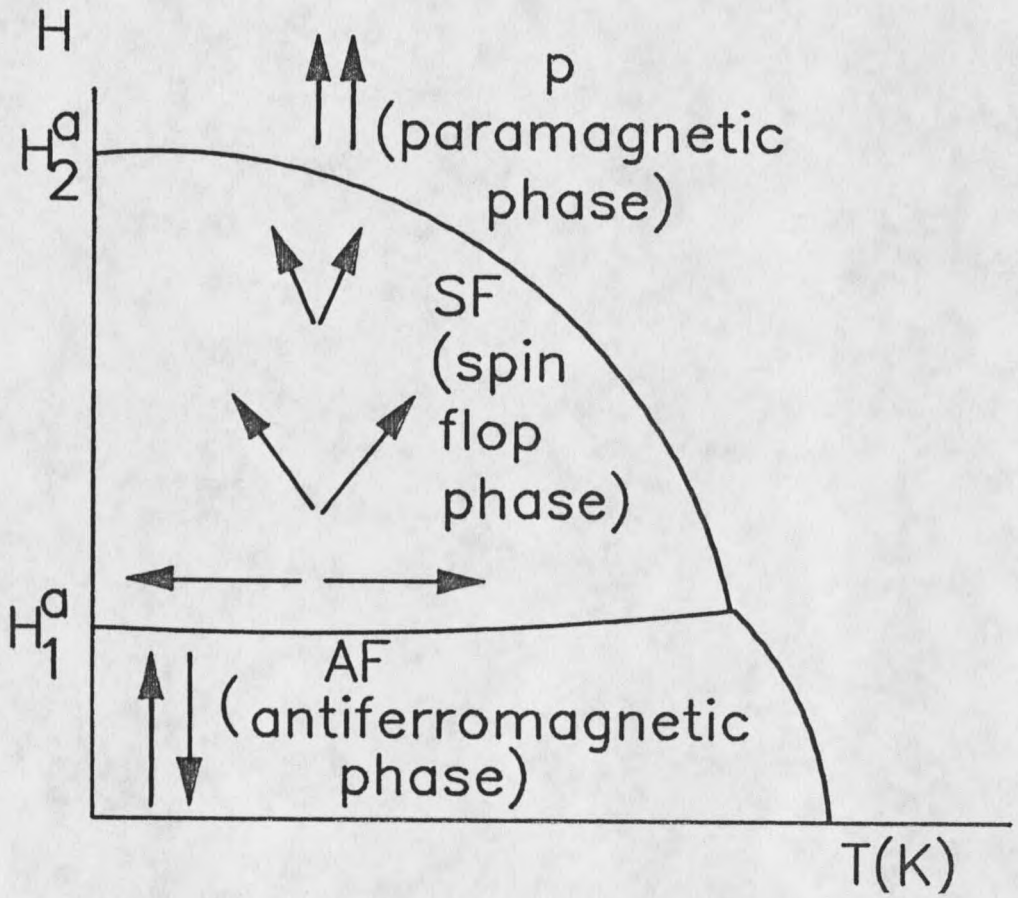

Figure 5. Phase diagram for an antiferromagnet with small anisotropy. The external field is applied parallel to the easy axis

This figure illustrates three distinct phase boundaries. These are: 1] paramagnetic [P] to antiferromagnetic [AF]; 2] AF to spin-flop [SF]; and 3] SF to P phase boundaries. When a field is applied along the easy axis of an antiferromagnet, a competition is set up between the applied field and the internal field, causing $T_c[H_a]$ to drop to a lower value as H_a increases. This is a second order phase transition and forms the P-AF phase boundary.

If an increasing field is applied, at a constant temperature below the Neel temperature, along the easy axis of an antifeorrmagnet, nothing will happen until the applied field becomes equal to that of anisotropy field. When the applied field slightly exceeds the anistropy field, the moments flop [nearly] perpendicular to the direction of the field. The field at which moments flop, is called spin-flop field. The transition is first order and this is a thermodynamically favored state. This forms the AF-SF phase boundary. A second order transition occurs when the moments line up with the field and the system enters into a paramagnetic state [SF-P transition].

Next we will drive the zero-T critical field by the method of mean field calculation and follow closely the format given by Drumheller, Rafaelle, and Baldwin (6).

The spin-Hamiltonian for a two-sublattice antiferromagnet can be written

$$H=-g\mu_B H\cdot S_i+2J\sum S_i\cdot S_j+LS_{iz}^2 . \qquad (1)$$

The first term is the Zeeman term. The second term represents the antiferromagnetic interaction between S_i and S_j. The exchange energy,

J, is assumed to be positive. The third term indicates the z-axis is the hard axis. We will subdivide the lattice of magnetic atoms into two sublattices, A and B, such that sublattices A and B point in opposite directions. According to the molecular field theory all magnetic atoms are identical and equivalent and S_k can be replaced by its average value <S>. Then the energy of Equation (1) can be written:

$$E = - (1/2)\, g\mu_B H\cdot\langle S_A\rangle - (1/2) g\mu_B H\cdot\langle S_B\rangle + Jn\langle S_A\rangle\cdot\langle S_B\rangle + L\langle S_z^2\rangle \qquad (2)$$

where n is the number of the nearest neighbor ions. We will use the coordinate system shown in Figure 6. The angle between sublattice spins and the hard axis (z-axis) is defined as θ. Energy for the AF phase, from Equation (2) is

$$E_{AF} = - JnS^2, \qquad (3)$$

For simplicity, we have written S for <S>. For the spin flop phase, Equation (2) becomes

$$E_{SF} = - g\mu_B HS \sin\theta - JnS^2 \cos 2\theta + LS^2 \cos_2\theta \qquad (4)$$

since E_{SF} is a function of θ,it can be minimized by setting $dE/d\theta = 0$. This gives

$$\sin\theta = g\mu_B HS/(4JnS^2 - 2LS^2). \qquad (5)$$

From Equation (5) cosθ and cos2θ can be found. Substituting these into Equation (4) will result in

$$E_{SF} =[-(g\mu_B HS)^2-8(JnS^2)^2-4(LS^2)^2+12(LS^2)(JnS^2)]/4(2JnS_2-LS^2) \qquad (6)$$

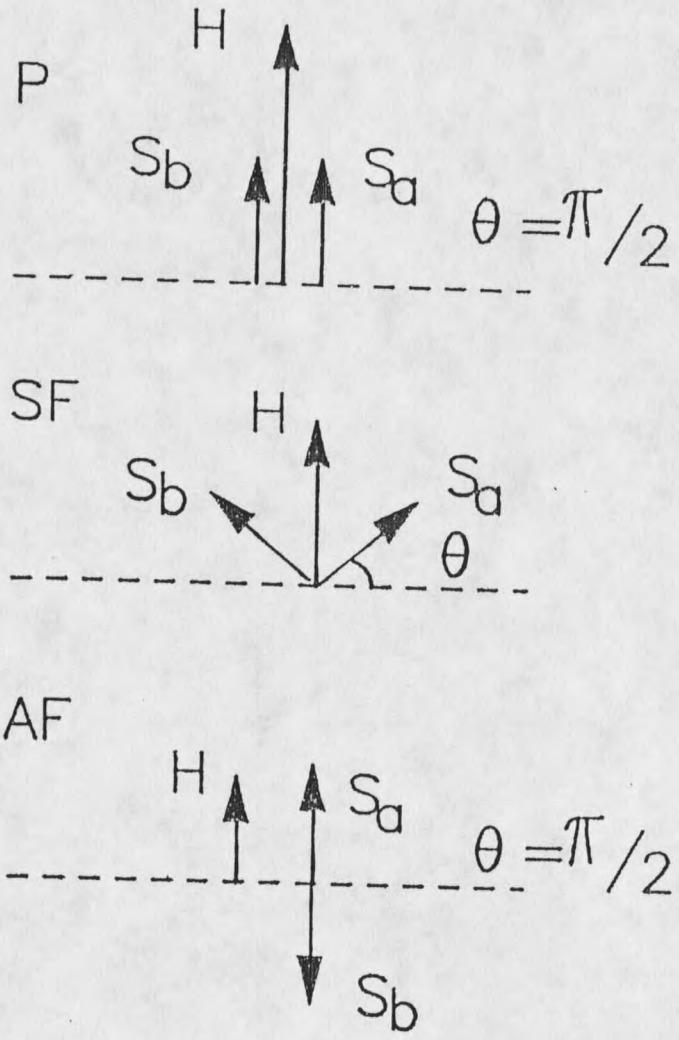

Figure 6. The coordinate system, discussed on page 14

At the spin-flop transition, Equations (6) and (3) are equal. This gives

$$(g\mu_B HS)^2 = 4[(2LS^2)(JnS^2) - (LS^2)^2], \tag{7}$$

dividing Equation (7)] by $(g\mu_B s)^2$, results in

$$H^2 = 2(2nJS/g\mu_B)\,(2LS/g\mu_B) - (2LS/g\mu_B)^2\,. \tag{8}$$

We define $H_{AF} = (2nJ/g\mu_B)$ and $H_A = (2LS/g\mu_B)$ and relabel H as H_{SF}, then Equation (8) becomes

$$H_{SF} = [2H_{AF}H_a - H_a{}^2]^{1/2}\,, \tag{9}$$

H_{SF} is the value of the antiferromagnetic to spin-flop transition field extrapolated to zero K. The field of the spin-flop to paramagnetic transition can be obtained by replacing θ by $\pi/2$ in Equation (5), this yields

$$H_c = 2H_{AF} - H_a\,. \tag{10}$$

These equations or appropriately similar ones will be used for our analysis in Chapter 5.

CHAPTER THREE

EXPERIMENTS

Sample Preparation

The $(C_2H_5NH_3)_2CuBr_4$ crystals were prepared by Professor K. E. Emerson of Montana State University. The ratio of the mole weight of $C_2H_5NH_3Br$ and $CuBr_2$ is two to one. Two parts of $C_2H_5NH_3Br$ and one part of $CuBr_2$ were dissolved in alcohol. The solution was filtered and put in a closed beaker in the presence of ether. By this method, good single crystals of fairly thin plates were obtained.

Crystal Structure

Although the crystal structure of $(C_2H_5NH_3)_2CuBr_4$ has not been solved in detail, dimensions of the unit cell and the distance between the copper-copper within the layer and between neighboring layers are known (Table 1). The crystal structure of known compounds of the $(C_nH_{2n+1}NH_3)_2CuX_4$ series are all orthorhombic with space group P_{bca}. These compounds consist of nearly isolated magnetic sheets of CuX_4 (X = Cl or Br), which are separated by two sheets of alkyl-ammonium groups. The cell constants a, b, and c for C_2Br are 7.9525, 7.7187, and 21.4191 Angstrom, respectively (7). Preliminary studies of this compound have shown that the unit cell is orthorhombic and the space group is P_{bca} (7).

The Vibrating Sample Magnetometer

Data were obtained using an EGG PAR Model 155 magnetometer. In addition to the magnetometer console and head, the system includes an electromagnet with field control and a cryostat with temperature control and measurement. The system is interfaced to an Apple II computer.

A schematic of the magnetometer head is shown in Figure 7 (8). It consists of the following: a mechanical vibrator, a long rod, a magnet, pick up coils, and a capacitor plate assembly. The sample is attached to the end of a long rod and placed between the pole faces of the magnet. The rod and the sample are vibrated perpendicular to the applied field by the mechanical vibrator at a frequency of 82.5 hertz. The magnetization of the sample induces a voltage in pick up coils placed on the magnet pole faces. The induced voltage has a frequency of 82.5 hertz and an amplitude proportional to the magnetization of the sample and to the amplitude of the vibration (9). The purpose of the capacitor is so that the detected voltage can be made independent of vibrational amplitude. A nickel standard is used to calibrate the magnetometer, since the saturation magnetization of nickel is known.

Temperatures over a range of 1.7 K to room temperature were controlled by both a current heater mounted below the sample and an adjustable gaseous flow rate. Temperatures at the lowest range were obtained by pumping on the sample chamber. The temperature was measured with a carbon glass resistor mounted directly above the

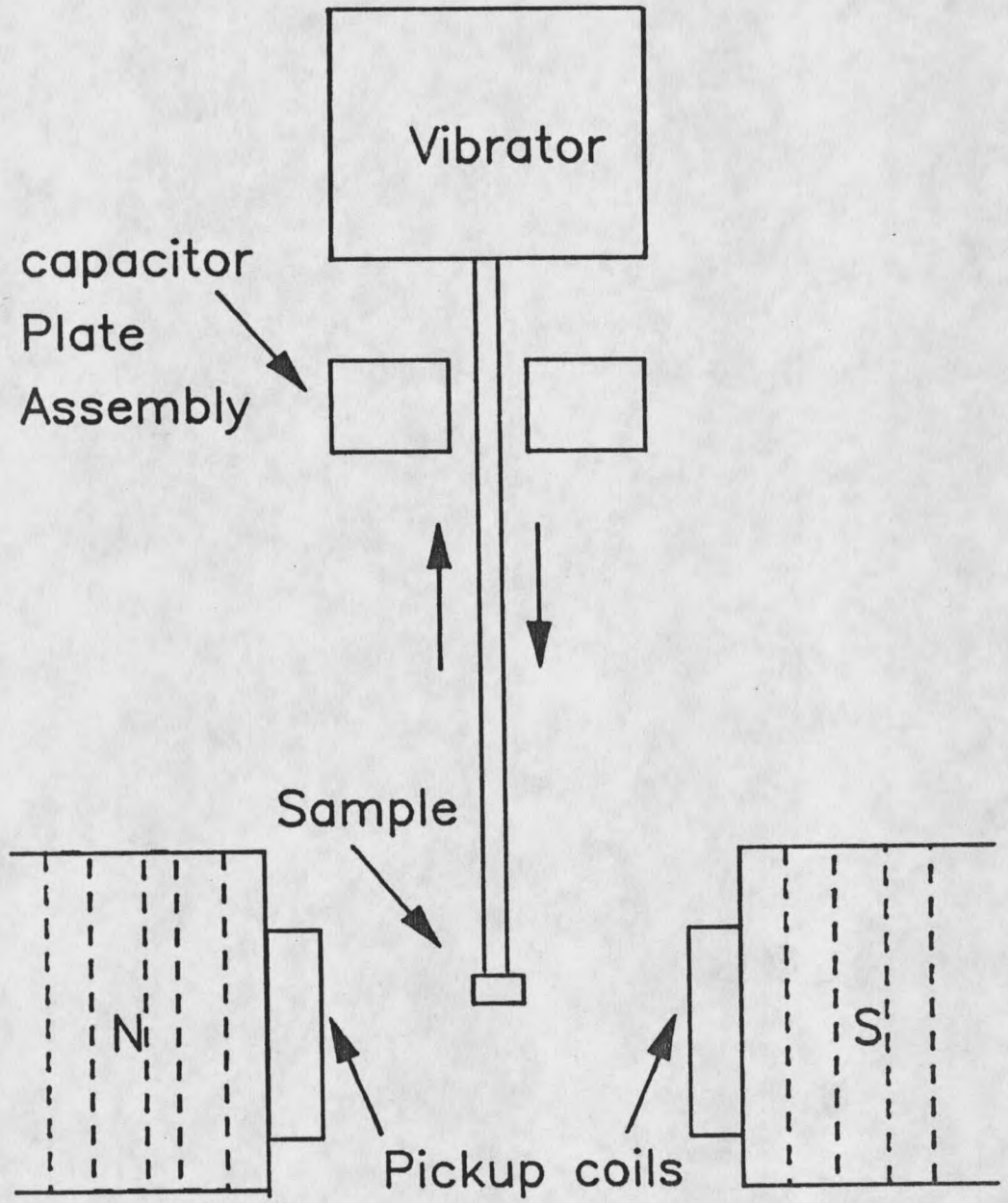

Figure 7. Schematic diagram of a vibrating sample magnetometer

sample. The stability of the temperature could be maintained within one mK at low temperatures and 0.1 K at room temperature.

A Walker/Magnion laboratory electromagnet with a 3 1/2 inch pole gap was used to provide magnetic fields of (-)5500 Oe to (+)5500 Oe. A Bell model 160 Gaussmeter measured and displayed the applied field.

Powder Measurements

Susceptibility versus temperature measurements were done on 133 mg of powder. The applied field was kept constant and temperature was varied from 20 K down to 4 K. Figure 8 shows the results of the susceptibility measurements for fields of 100, 500, and 1,000 Oe. Below the critical temperature the susceptibility increases abruptly and exhibits a strong dependence on the field. Note that in contrast to antiferromagnets, susceptibility in this system does not decrease below the critical temperature; instead it increases with a very small slope. This is due to the presence of a ferromagnetic moment.

In Figure 9, the molar susceptibility measurement in the high temperature region ($T>T_C$) with a field of 4000 Oe is presented. From this curve the exchange constant, J/k, and Curie constant, C, are derived and consequently a value for g_{powder} is given.

In the paramagnetic region, but at low temperatures, the susceptibility is dominated by the ferromagnetic intra-layer exchange interaction. The experimental data (shown by o) have been fitted to the simple quadratic Heisenberg model given by: Figure 10

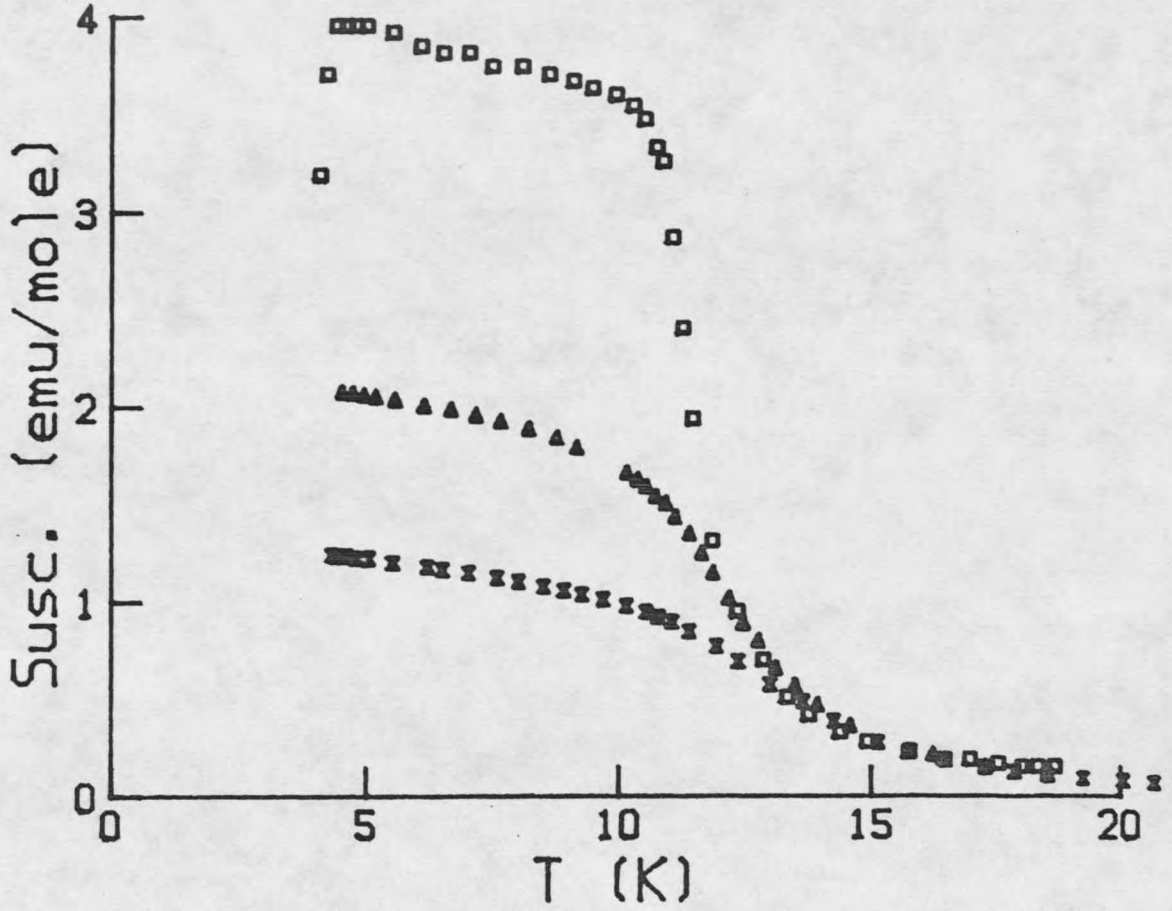

Figure 8. Temperature dependence of the molar magnetic susceptibility ofpowdersample at different fields

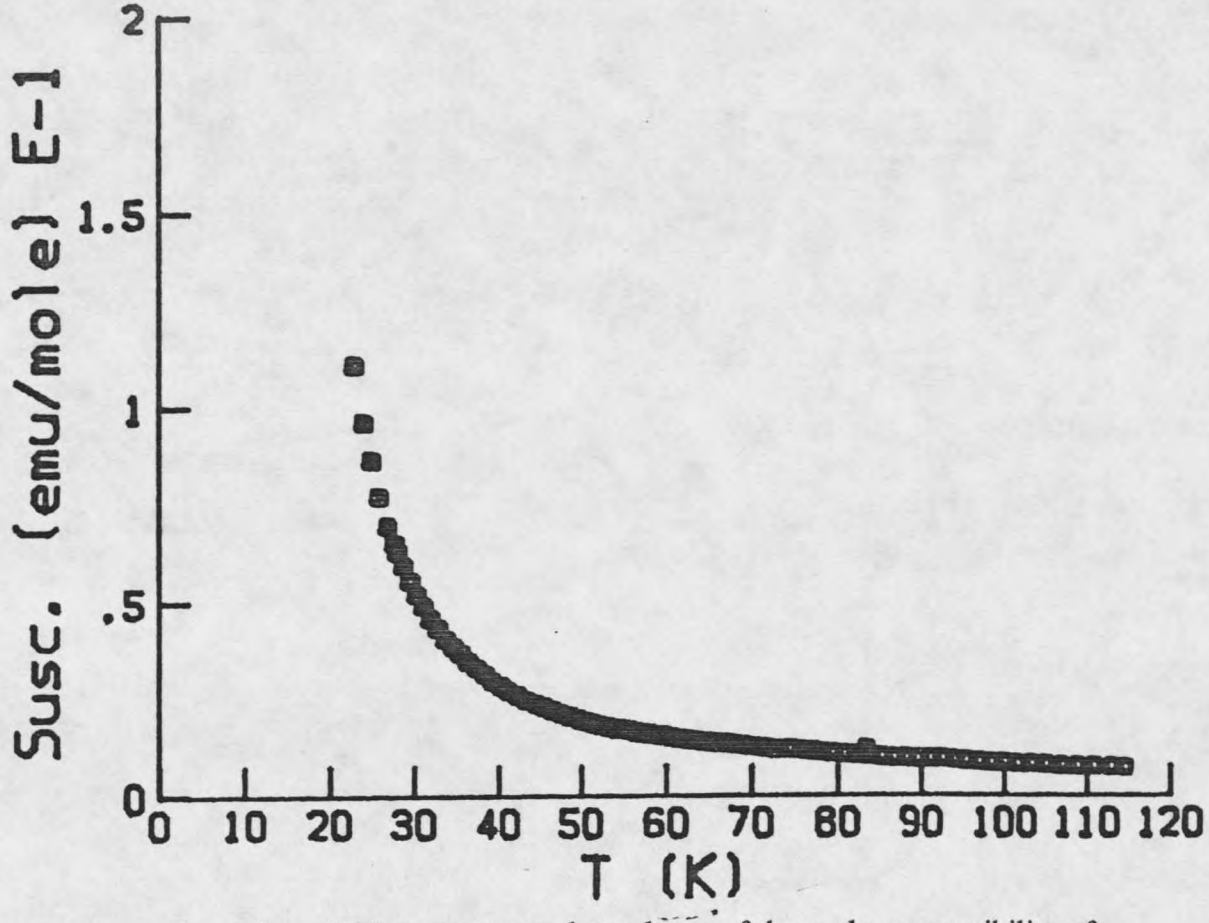

Figure 9. High temperature dependence of the molar susceptibility of powder sample at H = 4000 Oe

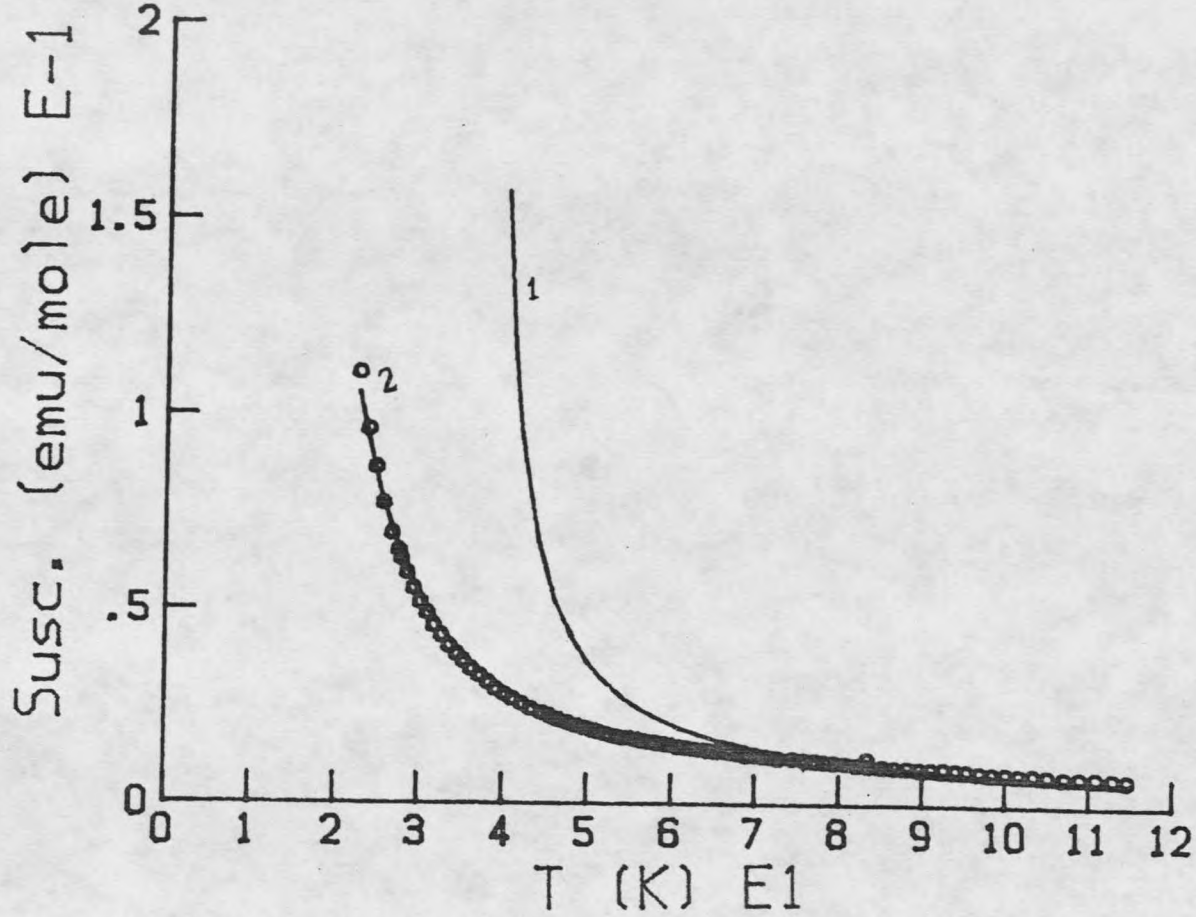

Figure 10. Powder susceptibility versus temperature. 1: Molecular field prediction 2: Simple quadratic Heisenberg model prediction o: Experimental data point

$$\chi T/C = 1 + \theta/T + (1/2)(\theta/T)^2(1\text{-}2e\text{-}1.5e^2) + (1/6)(\theta/T)^3(1\text{-}9e\text{-}7.875e^2$$

$$\text{-}1.125e^3) + (13/197)(\theta/T)^4(1\text{-}15.7e\text{-}6.7e^2 + 7.6e^3 + 3.14e^4).$$

The Curie-Weiss temperature, θ, is related to the intra-layer exchange interaction by $J_1 = (\theta/2)(1+e)$. e and θ are related to the inter-layer exchange interaction by $J_2 = -(1/4)\theta e$. Since J_2 is very small it could not be obtained from the above equation. The theoretical curve, also obtained from the above Equation, is shown by a full line drawn through the experimental points. Since only a finite number of terms are known in the high termperature series expansion, Equation (1) can only represent χ in a certain temperature range. Equation (1) was used for

$$J/kT \leq 0.66 .$$

The best fit to the theoretical curve gives a result of

$$J/k = 18.5 \text{ K}; \; C = 0.45 \text{ emu-K/mole and } J/kT_c = 1.72.$$

Using the experimental value of C and the equation

$$C = Ng^2\mu_B J(J + 1)/3k ,$$

a value of 2.25 for g_{powder} is obtained. A positive Curie-Weiss temperature, q , of 37 K is the result of this fitting which is indicative of ferromagnetic interaction in the plane. The reported values for J/k and J/kT_c are 19.0 K and 1.72 , respectively, which agree with our results.

Also plotted in Figure 10 are the molecular field results,

$$C/\chi T = 1\text{-}\theta/T$$

This is done to demonstrate the deviation from the molecular field result. As temperature decreases, χ deviates from the experimental data.

Coordinate System

Magnetization versus field measurements at a constant temperature below the ordering temperature were carried out in an attempt to establish a coordinate system. The sample on which measurements were taken was a dark platelet of dimensions 3.5 x 4.5 x 0.2 mm^3, with a mass of about 4.3 mg. An x-ray analysis at room temperature showed that the principal c-axis was perpendicular to the face of the plate. Figure 11 shows the result of the measurement of the magnetic moment as a function of the applied field at T = 5.5 K. The magnetization curves are represented by Hcϕ where ϕ is the angle between the c-axis and the appied field, H,. Figure 11 discloses a minimum magnetization for ϕ = 90 degrees and maximum for ϕ = 0 degrees. In the future we shall use a coordinate system in which the z-axis is parallel to the c-axis and the y-axis is parallel to the Hz90 direction. The x and y axes make a plane parallel to the face of the plate.

Susceptibility Versus Temperature

The single crystal magnetic susceptibility of $(C_2H_5NH_3)_2CuBr_4$ shows an anisotropy, with different behavior for each principal axis susceptibility. Susceptibility data were obtained with the applied field along the y, z, and x axes. Single crystal magnetic susceptibility data for C_2Br, with an applied field along y, z, and x axes for temperatures between 4 K and 20 K are shown in Figures 12, 13, and 14

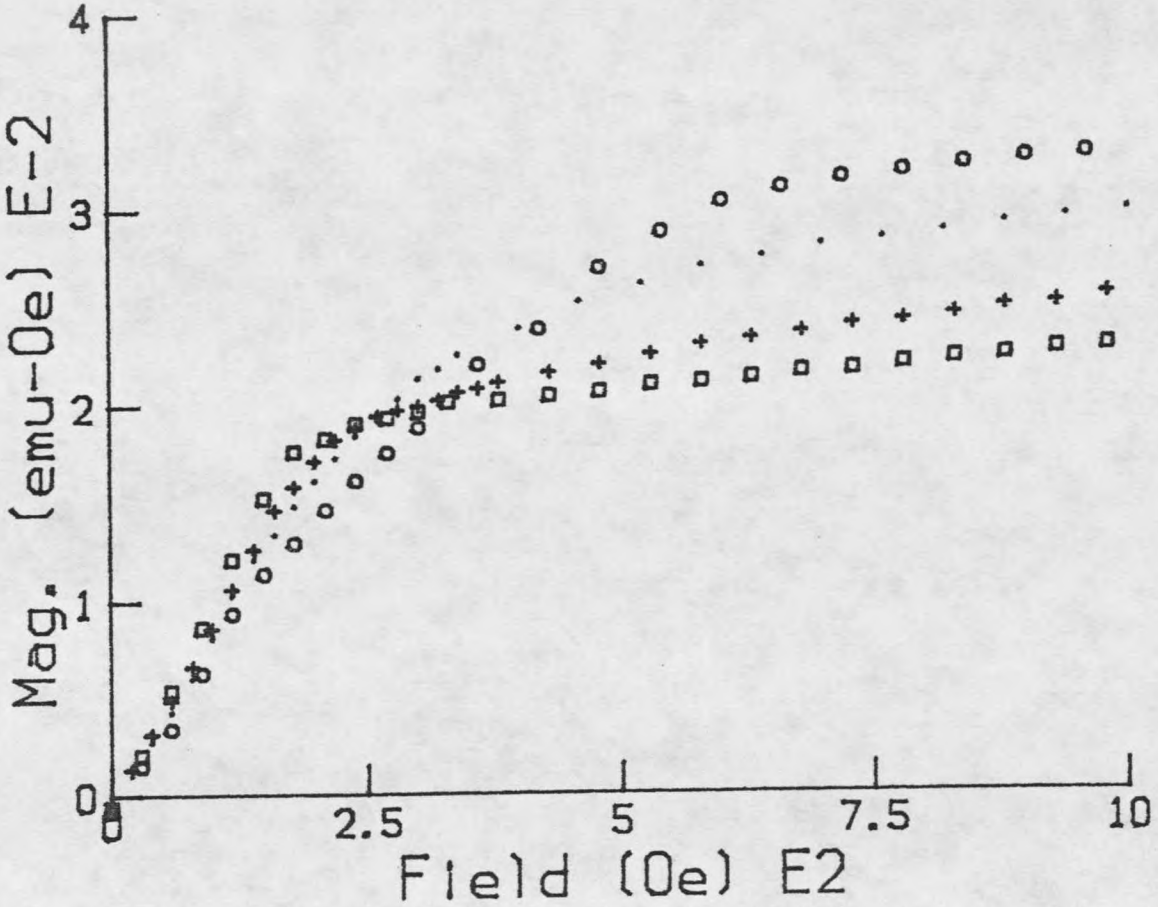

Figure 11. The magnetic moment, m, as a function of applied field, H,at T = 5.5 K. The upper curve represents field along the y-axis and the lower curve represents field along the z-axis

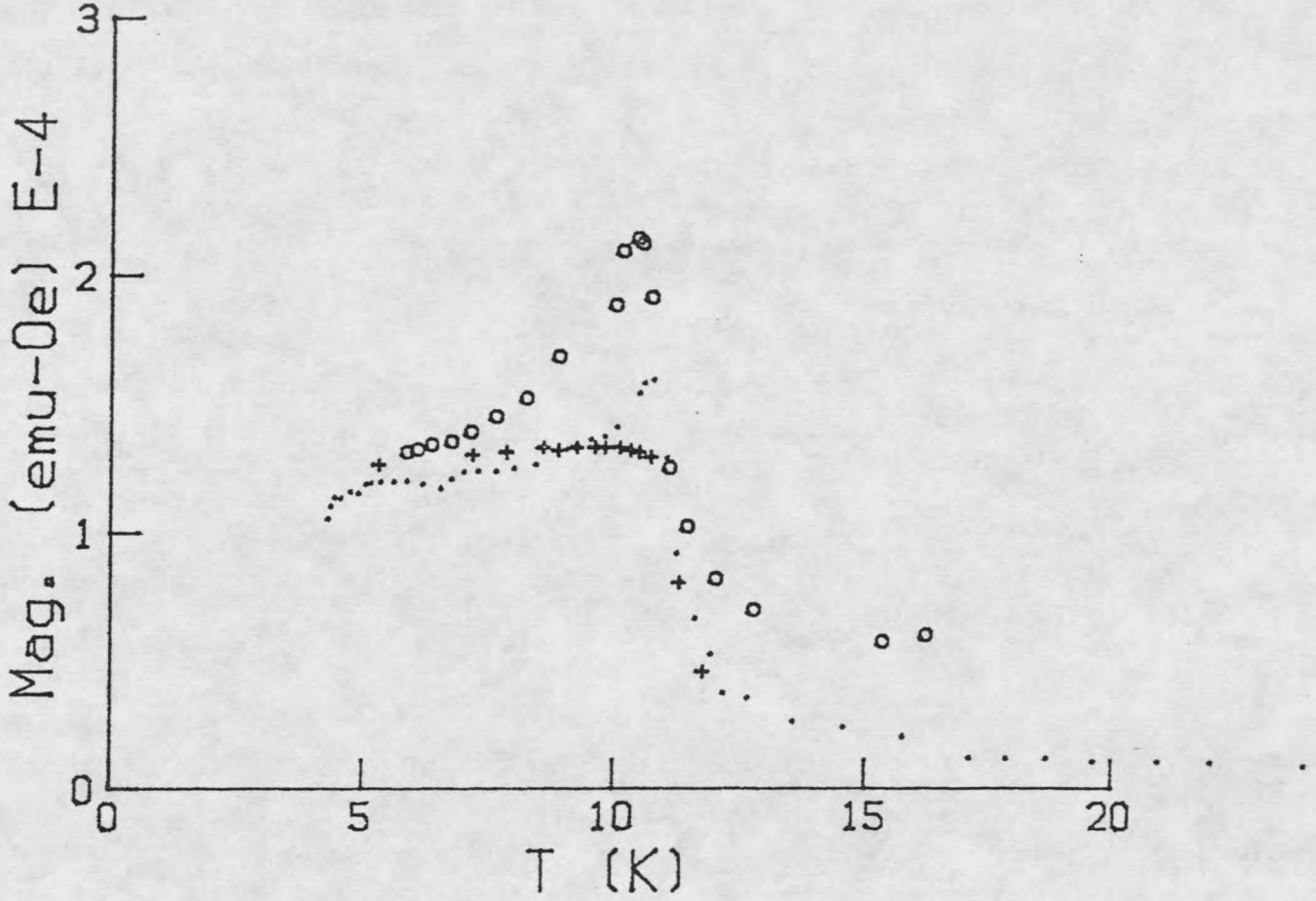

Figure 12. Magnetic susceptibility measured parallel to the y-axis at low temperatures (circle, 10 Oe; dot, 40 Oe: plus, 100 Oe)

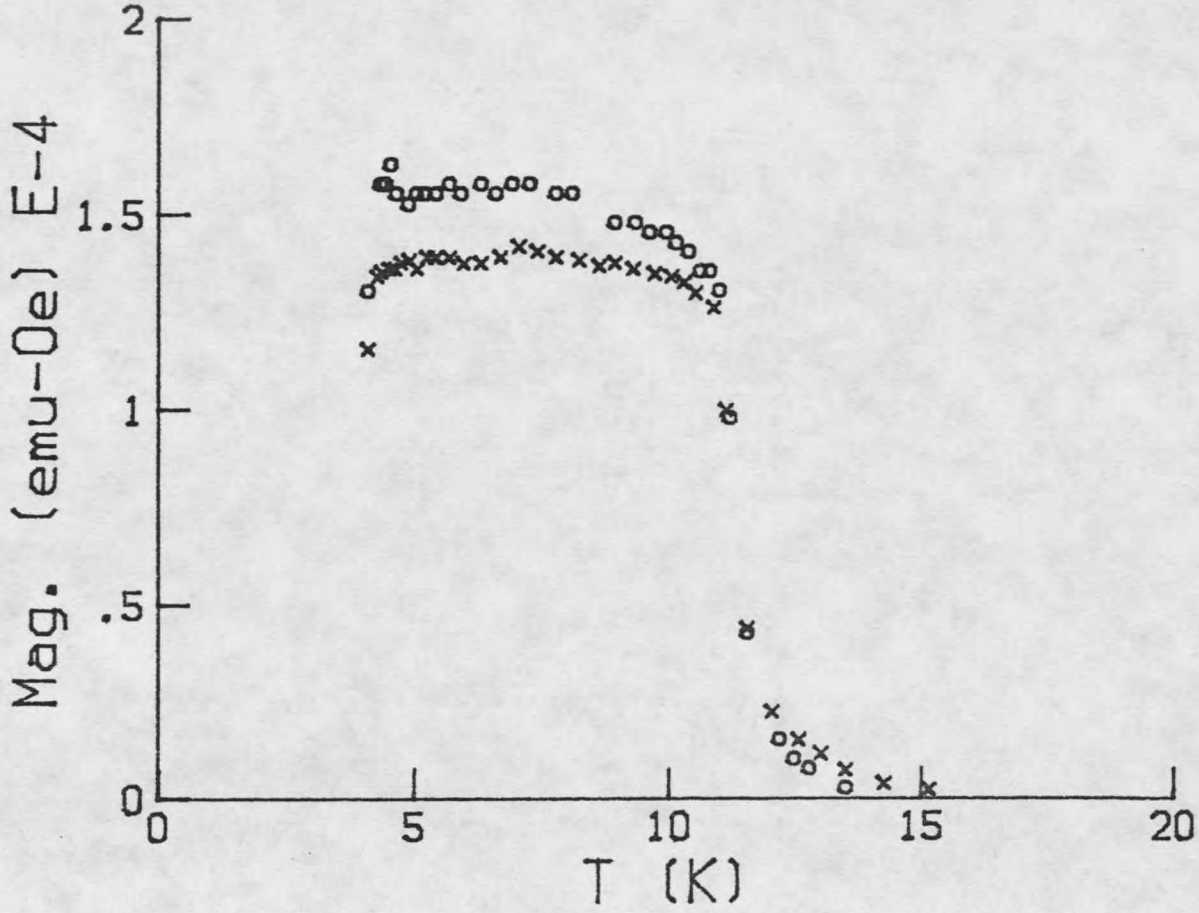

Figure 13. Magnetic susceptibility measured parallel to the z-axis at low temperatures (circle, 20 Oe; cross, 70 Oe)

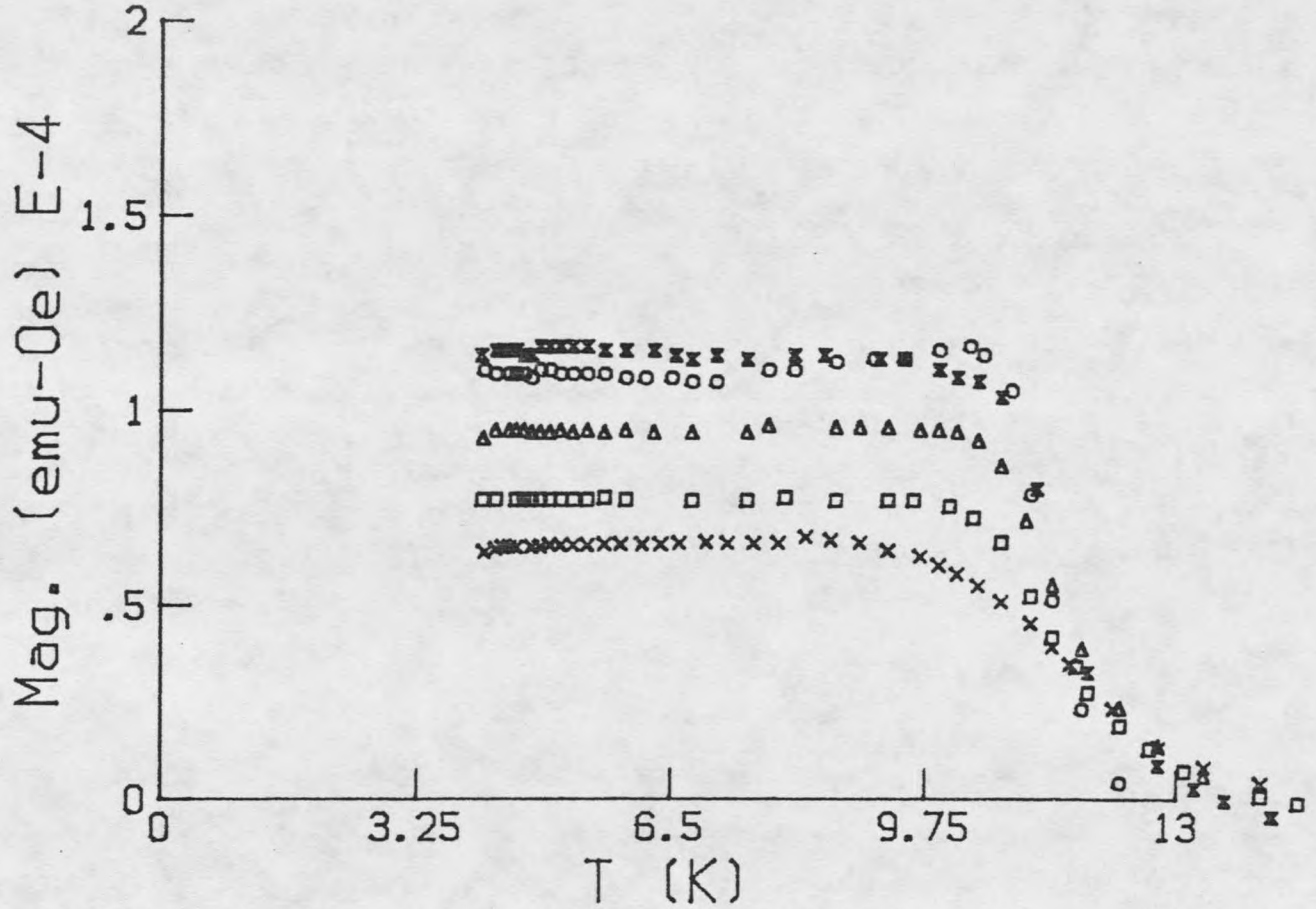

Figure 14. Magnetic susceptibility measured parallel to the x-axis at low temperature (circle, 50 Oe; dbl.tri., 100 Oe; triangle, 150 Oe; square, 200 Oe; cross, 300 Oe)

respectively. Figure 12 shows susceptibility data taken at constant fields. The crystal was oriented so that the applied field was parallel to the y-axis. Of particular interest are the susceptibility data collected below 100 Oe. At the field of 10 Oe, χ_y passes through a pronounced maximum near T_N = 10.75 ± 0.05K, and falls off rapidly down to T = 7 K. The graph in Figure 12 identifies C_2Br as a weak antiferromagnet with a Neel temperature of 10.75 ± 0.05 K. With increasing magnetic field T_N shifts to lower temperatures and finally disappears at a field of 100 Oe. The fact that T_N has almost disappeared at 100 Oe, suggests that the critical field is less than 100 Oe. Note that in contrast to the classical antiferromagnet, the susceptibility here does not approach zero as temperature approaches zero. This is a further indication of the presence of a weak ferromagnetic moment. Figures 13 and 14 show the susceptibility as a function of temperature along the z and x-axes, respectively. The susceptibility along the z-axis has not been corrected for demagnetizing effects. The susceptibility remains constant below the transition temperature. When the field is applied along the x-axis, the susceptibility at the field of 50 Oe exhibits a small peak. The source of this peak can be the misalignment of the crystal or perhaps, the presence of weak ferromagnetic moment.

Magnetization versus Field

Magnetization measurements were carried out on a single crystal along x, y, and z axes from zero applied field to about 5500 Oe at temperatures below the transition temperature. Figure 15 shows the expanded scale (0 - 1000 Oe) measurements of the magnetic moment as a

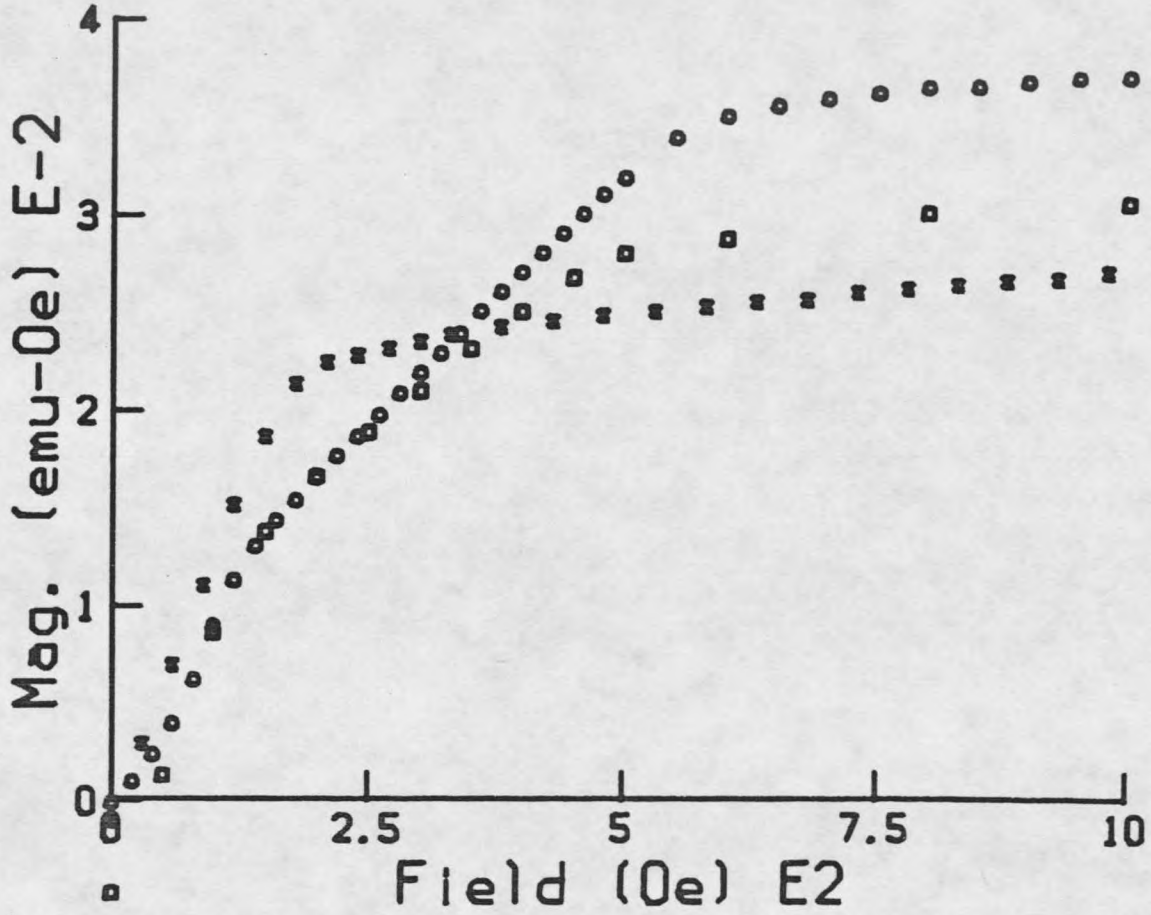

Figure 15. Magnetization versus field at 4.8 K along x,y, and z axes (circle, y-axis; square, x-axis; cross, z-axis)

function of the applied field at T = 4.8 K. This figure clearly reveals the existence of out-of-plane anisotropy. It should be noted that when the field was applied parallel to the x or y-axes, the demagnetizing factor was assumed to be zero, since the crystal plate was fairly thin. Measurements along the z-axis have been corrected for the demagnetizing field according to

$$H = H_a - 4\pi DM \quad ,$$

where demagnetizing factor D is assumed to be 0.8 and H_a is the applied field. The data represented by circles is obtained when the field is applied along the y-axis. The diagram shows that the dependence of the magnetic moment on the field, for 150 <H <600 Oe can be described by

$$M_y(H,T) = \sigma(T) + \chi_y(T)H_y$$

where $\sigma(T)$ is the ferromagnetic moment and is obtained by extrapolation to zero field. From magnetization versus field curves, the temperature dependence of $\sigma(T)$ is determined as shown in Figure (16). It has the form characteristic of an ordering curve except for an anomalous behavior at T=5.2 K. Similar behavior of $\sigma(T)$ has been observed in $CoCO_3$ (10). When the applied field has reached 650 Oe, magnetization is effectively saturated. In weak fields, to be precise at 80 ±5 Oe, an anomaly is observed. This discontinuity in magnetization at the anomaly field is characteristic of a first order transition. As is seen from the diagram, the dependence of magnetic moment on applied field differs from that of a classical antiferromagnet. Magnetization does not remain constant up to the field at which the anomaly occurs, but increases with

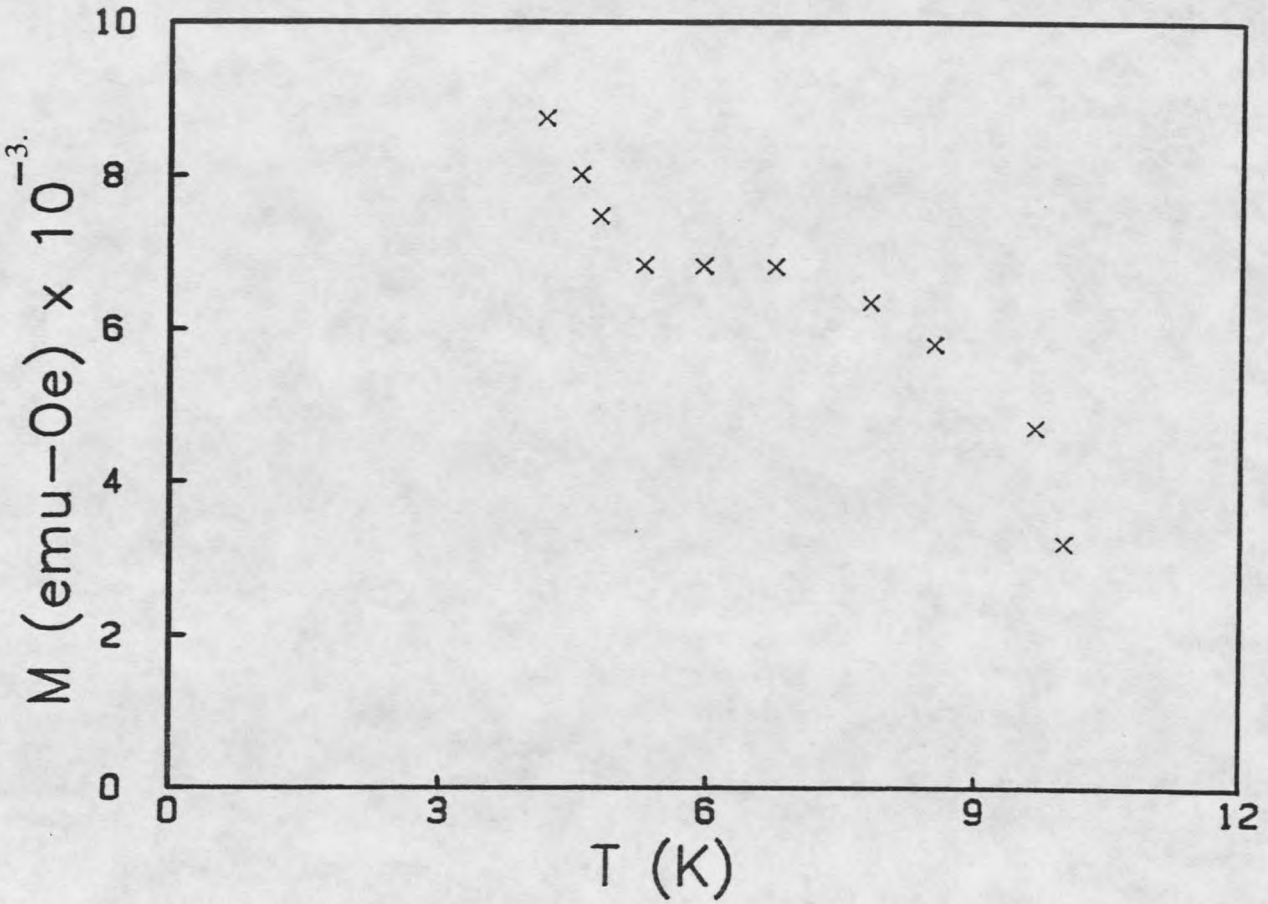

Figure 16. Temperature dependence of weak ferromagnetic moment

some slope. An expanded scale (0 - 200 Oe) of magnetization versus field at temperatures between 1.85 K and 10.5 K is shown in Figure 17. The isotherms exhibit more rounding above and below the anomaly field, the value of which remains constant as temperature rises. The data indicated by squares represents magnetization versus field along the x-axis at T = 4.8 K. The dependence of magnetization on the applied field along this direction indicates that ferromagnetic moment is being rotated toward this axis. The field variation of the magnetization along the z-axis is represented by crosses. In weak fields, H < 150 Oe, the magnetic moment changes linearly with the field according to

$$M_z = \chi_z H_z \ ,$$

like in an ordinary paramagnet. This curve was found to be completely reversible as shown in Figure 18.

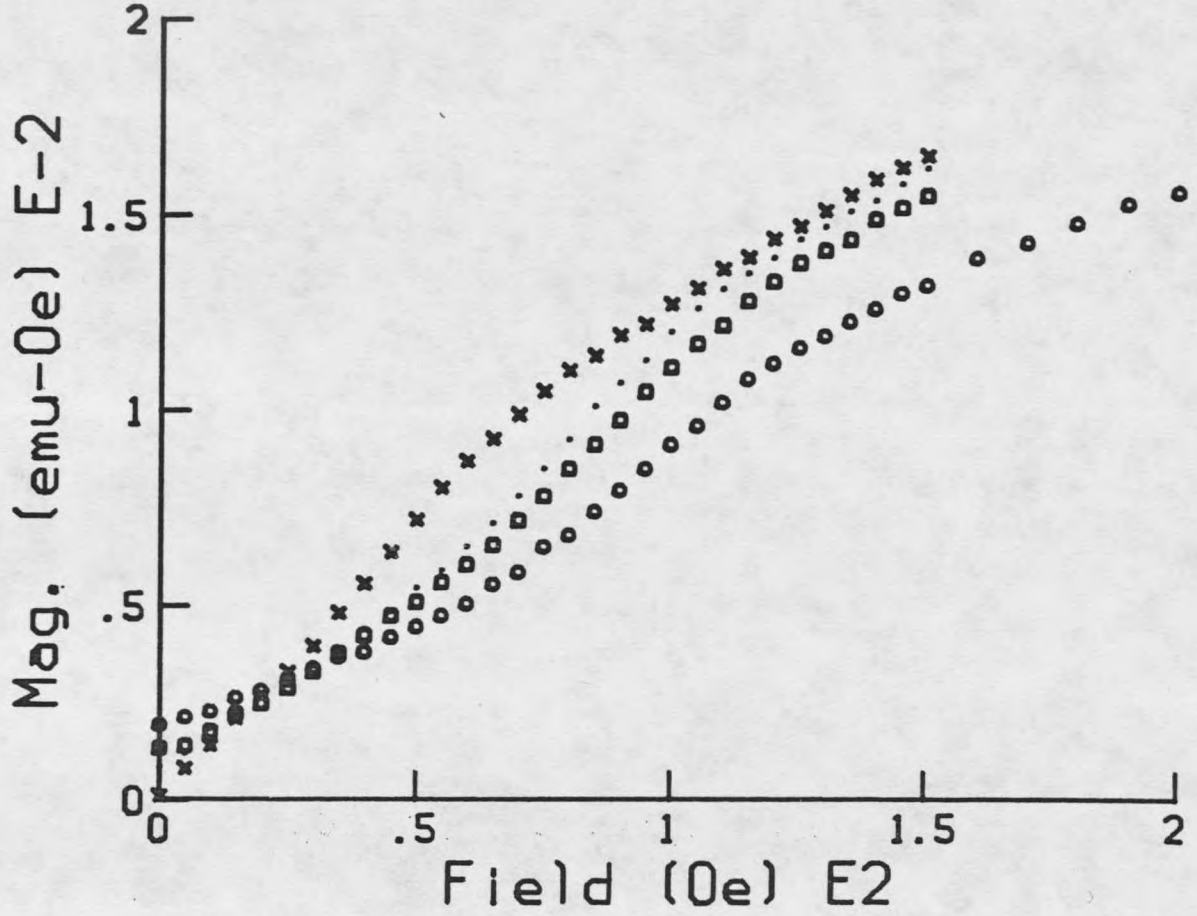

Figure 17. The magnetization versus applied field for several temperatures (cross, 10.5 K; dot, 6 K; square, 4.4 K; circle, 1.85 K)

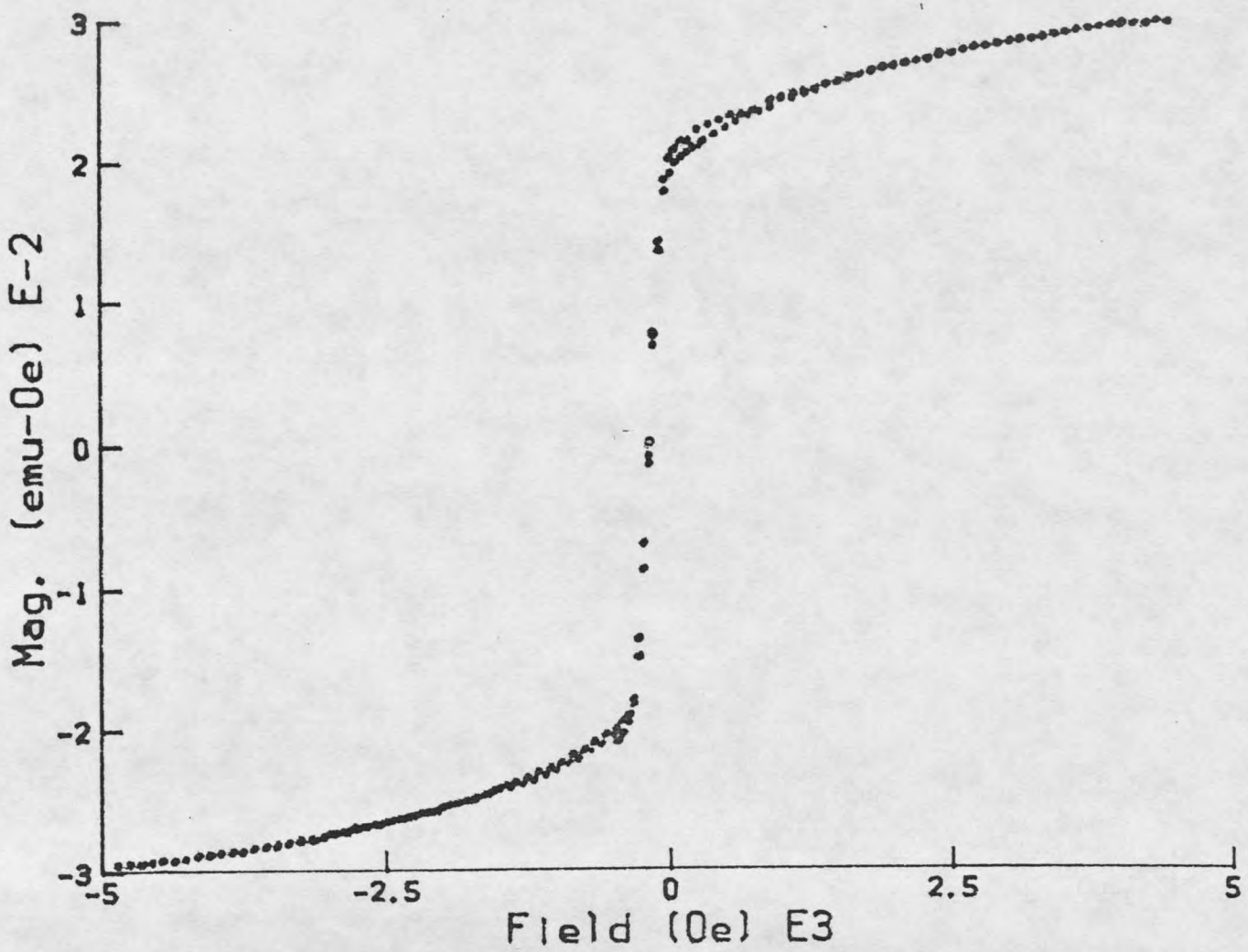

Figure 18. Hysteresis loop of C_2Br, field is applied along the z-axis

CHAPTER FOUR

MEAN FIELD CALCULATION

In this chapter the critical parameters are presented which have been determined by means of mean field calculations.

The basic idea of the mean field model is that if spins i and j are localized on sites i and j, then the interaction between them can be represented by the form of

$$E_{ex}=-2J_{ij}\vec{S}\cdot\vec{S}_j \qquad (1)$$

where J_{ij} is a function of the relative separation between spins i and j. The exchange parameter J_{ij} is positive if the spins i and j are parallel, and if J_{ij} is negative anti-parallel alignment of spins are energetically favored. The most general form of Equation (1) can be written as (11)

$$E=\vec{S}_i\cdot K_s\cdot\vec{S}_j+\vec{S}_i\cdot K_a\cdot\vec{S}_j \qquad (2)$$

where K_s and K_a are symmetrical and antisymmetrical tensors. If the element of K_a and K_s are different, then we have anisotropic exchange interaction. In an antiferromagnetic system, the symmetrical part of Equation (2) assumes minimum energy when spins are ordered antiferromagnetically. Therefore, in the most favorable condition (H = 0 and T = 0) the symmetrical part of Equation (2) cannot give rise to the canting of the spins. The antisymmetric part of Equation (1) is expressed by a form(11)

$$\vec{d} \cdot [\vec{S}_i X \vec{S}_j] \qquad (3)$$

where d is a constant vector. Equation (3) is minimum when spins are 90 degrees apart. Therefore, an antiferromagnetically ordered system can be canted by the presence of a term such as (3). The antisymmetric part of the exchange interaction can exist if the g tensors of the two ions are different, or the crystal symmetry is low. In the case of C_2Br, the crystal symmetry is sufficiently low, therefore presence of such a term is expected in the free energy expression. The physical origin of the antisymmetric part of Equation (3) is a combined effect of the spin-orbit coupling and the exchange interaction.

Expression for Free Energy at Zero Kelvin

In this section an expression for free energy at zero K is given. Effective parameters have been determined by mean field theory fitted to experimental data.

Figure 19 shows the copper ion sites in a unit cell. Spins [1] and [2] are located within a plane and spins [3] and [4] are located in the next plane. Yoshio proposes a spin structure, shown in Figure 20, as a result of his NMR studies at zero field and T = 1.7 K. The suggested spin structure is indicated by the arrows. The moments lie in the bc plane and are canted toward the c-axis (Yoshio).

If the Yoshio model is correct, then the magnetization versus applied field measurements along the z-axis should reveal a net moment

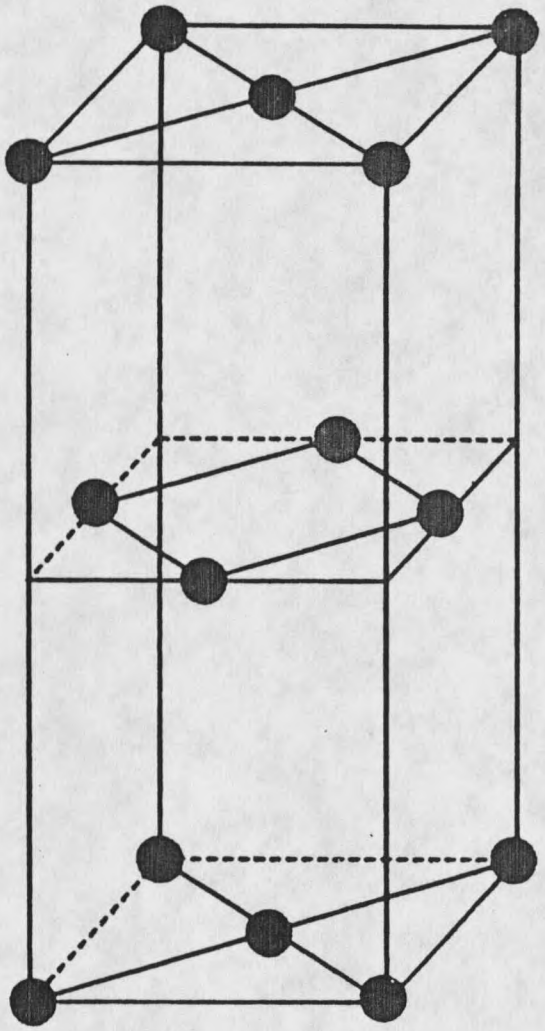

Figure 19. Unit cell of C_2Br, only copper ions are show

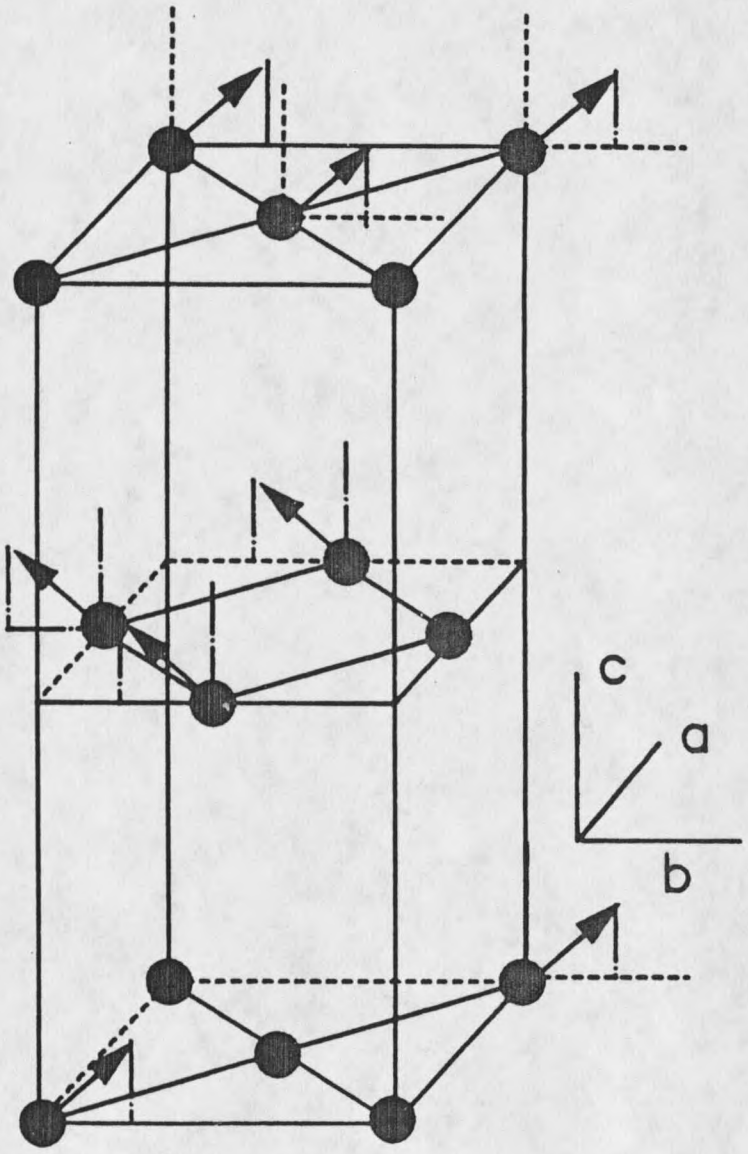

Figure 20. Spin structure for C_2Br suggested by Yoshio

at zero field, see Figure 15. Furthermore, application of the field along this axis revealed the absence of domains, see Figure 18. The possible explanations for the absence of domain and zero net moment are the following:

I) A four sublattice magnet: the possible spin structure of the four-sublattice antiferromagnet is shown in Figure 21. The antiferromagnetic exchange field, H_{AF}, couples spins (1) and (3) (or 2 and 4). Furthermore, the antiferromagnetic moments tilt in the bc plane at the angle θ with the c-axis in zero applied field. We could not fit our experimental data and get reasonable results to this model.

II) A covert weak ferromagnet: at zero field and zero temperature, spins are located within the plane, possibly along the [110] direction because the crystal is distorted along this direction (12). When an external field of a few Oersted is applied within the plane, the competition between the terms in the free energy leads to a tilting of the spins in the yz plane. Note that $(C_2H_5NH_3)_2CuCl_4$ is a covert weak ferromagnet (13).

III) A soft magnet: a material is called a soft magnet if coercive force is smaller than 5 Oe. Coercive forces as small as 10^{-3} Oe have been observed (Moorish). We assume that the domain walls are plane and parallel to the z-axis. Consider one such a wall; if a magnetic field H is applied parallel to the z-axis then the wall will tend to be displaced, as indicated in Figure 22. The field required to produce this displacement is very small. Therefore, a single crystal will possess a very small coercive force. So, it would be reasonable to see no hysteresis along the z-axis.

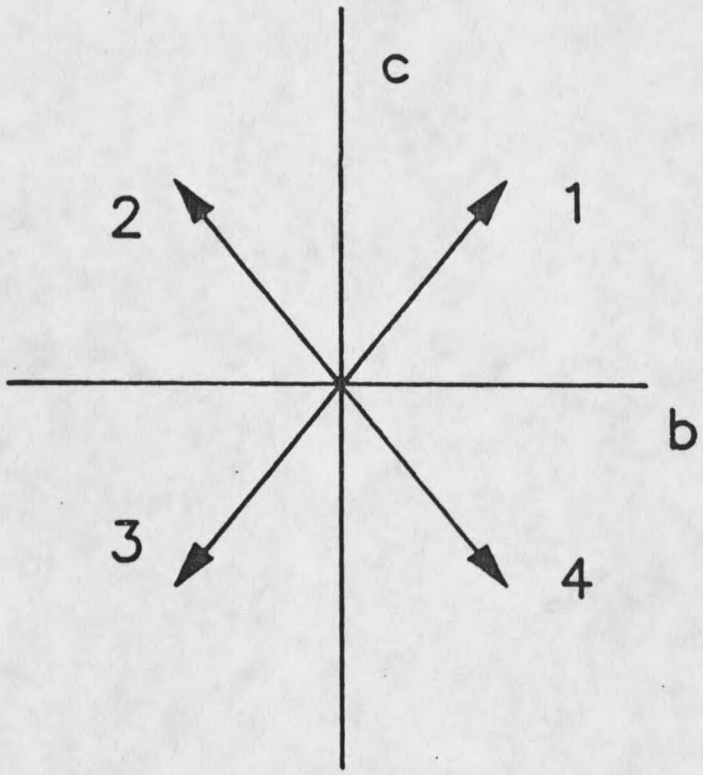

Figure 21. Four-sublattice magnet at zero field

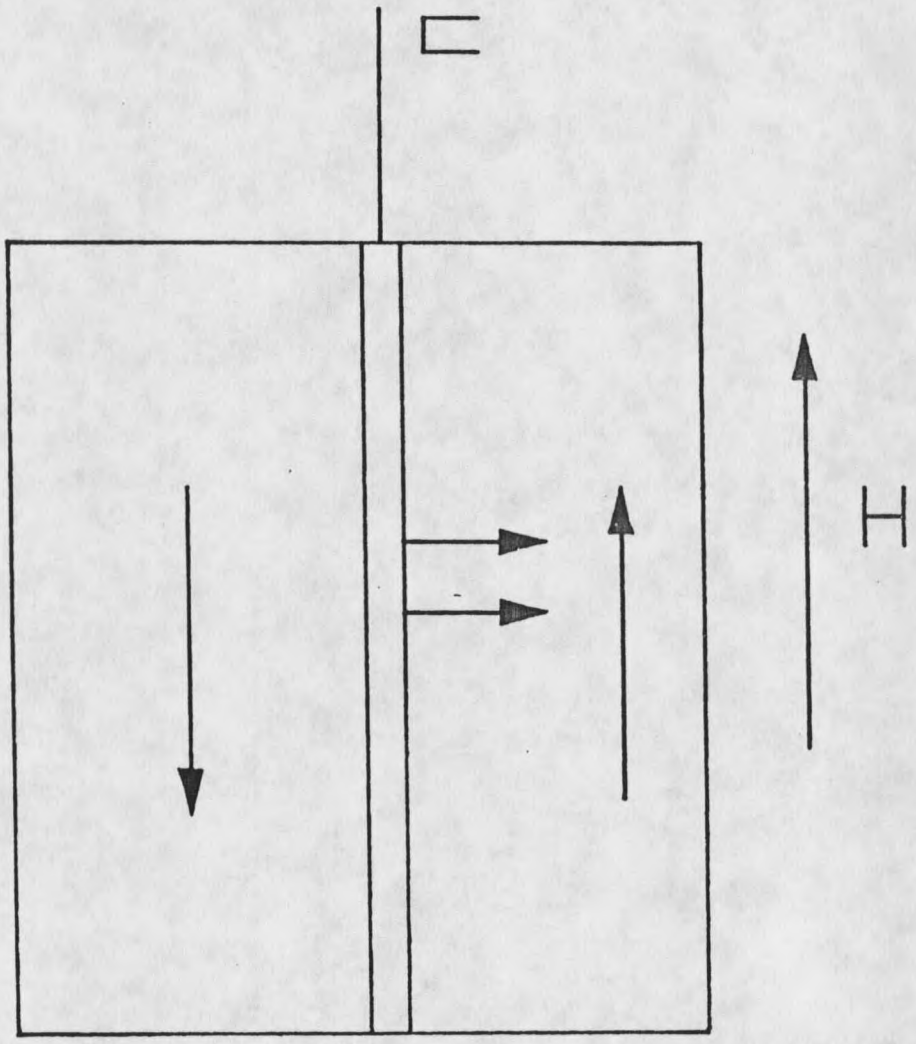

Figure 22. Domain wall movement in soft magnet

We cannot be absolutely certain which of the above explanations is correct. However, Yoshio's model, with the assumption that C_2Br is a soft magnet seems to fit our experimental data.

We will now describe our experimental data on the basis of two-sublattice magnet. The interaction Hamiltonian is given by Yoshio.

$$H = -2J\sum\{S_i^xS_j^x+S_i^yS_j^y+(1-J_a/J)S_i^zS_j^z\}$$

$$-2J\sum\{S_l^xS_m^x+S_l^yS_m^y+(1-J_a/J)S_l^zS_m^z\}$$

$$-2J'\sum S_j\cdot S_m$$

$$-2J_d\sum(S_i^yS_j^z+S_i^zS_j^y)+2J_d\sum(S_l^yS_m^z+S_l^zS_m^y)$$

$$-2J_d'\sum S_j x S_m$$

$$-g\mu_B H\cdot(\sum S_i+\sum S_l).$$

In the above, Hamiltonian terms are defined as follows:

1. i,j,l, and m are four copper sites, corresponding to 1,2,3, and 4 in Figure 20.

2. S_i, S_j, S_l, and S_m are the spin angular momentum vectors of atoms i, j, l, and m measured in units of $h/2\pi$ respectively.

3. J is the ferromagnetic exchange integral which has a positive sign.

4. J' is the antiferromagnetic exchange integral which is negative.

5. J_a is the anisotropic part of the exchange interaction, which includes the dipolar interaction and anisotropic exchange interaction.

6. J_d and $J_d^{|}$ are intra- and inter-layer anisotropy parameters responsible for the weak ferromagnetism.

7. g is the symmetric tensor.

8. The effective field parameters are defined by:

$$H_a = 2ZJ_AS/g\mu_b \text{ , } H_{AF} = 2Z^{|}J^{|}S/g\mu_b \text{ , } H_d = 2ZJ_dS/g\mu_b$$

$$\text{and } H_d^{|} = 2Z^{|}J_d^{|}S/g\mu_b$$

where Z and $Z^{|}$ are the number of nearest and next nearest neighbors. Furthermore, the values of H_d and $H_d^{|}$ are given by:

$$H_d = [((g-2)/2)^2]H_E \text{ , } \qquad H_d^{|} = [(g-2)/2]H_{AF}$$

with H_{AF} of the order of 1000 Oe and $H_E = 5.4 \times 10^5$ Oe $H_d^{|}$ amounts to less than 5% of H_d. Therefore, the $H_d^{|}$ term can be neglected. We assume that exchange integrals are the same for all the interacting neighbors and replace the sum ΣS_K by $Z\langle S_k\rangle$, where $\langle S_K\rangle$ means the statistical average of S_k over the sublattice to which k belongs and Z is the number of nearest neighbor ions.

Field Applied Along the Z-axis

We will adopt the coordinate system shown in Figure 23. α is the angle between spin S_i and the z-axis and spin S_l and the z-axis. If an external magnetic field is applied along the z-axis then the free energy can be written as:

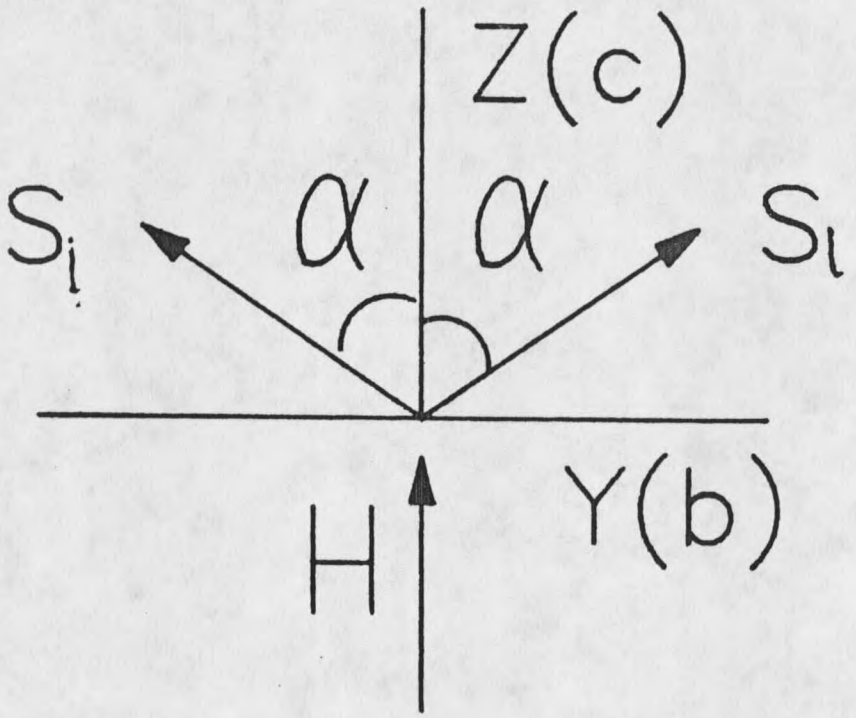

Figure 23. Spin configuration relative to the applied field

$$E/g\mu_B S = -2H_E + 2H_a\cos^2\alpha - H_{AF}\cos 2\alpha - 2H_d\sin 2\alpha - 2H\cos\alpha$$

Since free energy is a function of α it can be minimized by setting $dE/d\alpha = 0$. This gives

$$H\sin\alpha = (2H_{AF} + H_a)\sin 2\alpha + 2H_d\cos 2\alpha$$

In an attempt to obtain numerical values for $(2H_{AF}+H_a)$ and H_d the magnetization curve at a temperature of 3.87 K was fitted to the above equation by the method of least-squares fit.

The following values were obtained: $(2H_{AF} + H_a) = 2150 \pm 50$ and $H_d = 2600 \pm 50$ Oe. The results of the fitting is shown in Figure 24, where the full curve represents calculated values of the magnetization as a function of the applied field and the circles represent the experimental data. The agreement between two curves is good within the experimental error.

Field Applied Along the Y-axis

Let us apply an external field along the y-axis as shown in Figure 25(a). We define θ as the angle between the y-axis and spin i and Φ as the angle between the z-axis and spin 1. Furthermore, we define vectors m and l by $m = S_1 + S_i$ and $l = S_i - S_1$ as shown in Figure 25(b). If an increasing external field is applied along the y-axis the following situation will occur. The applied field will tend to rotate vectors m and l so that m is parallel to H and l is perpendicular to H. But, contrary to the expected outcome, vector m will suddenly orient

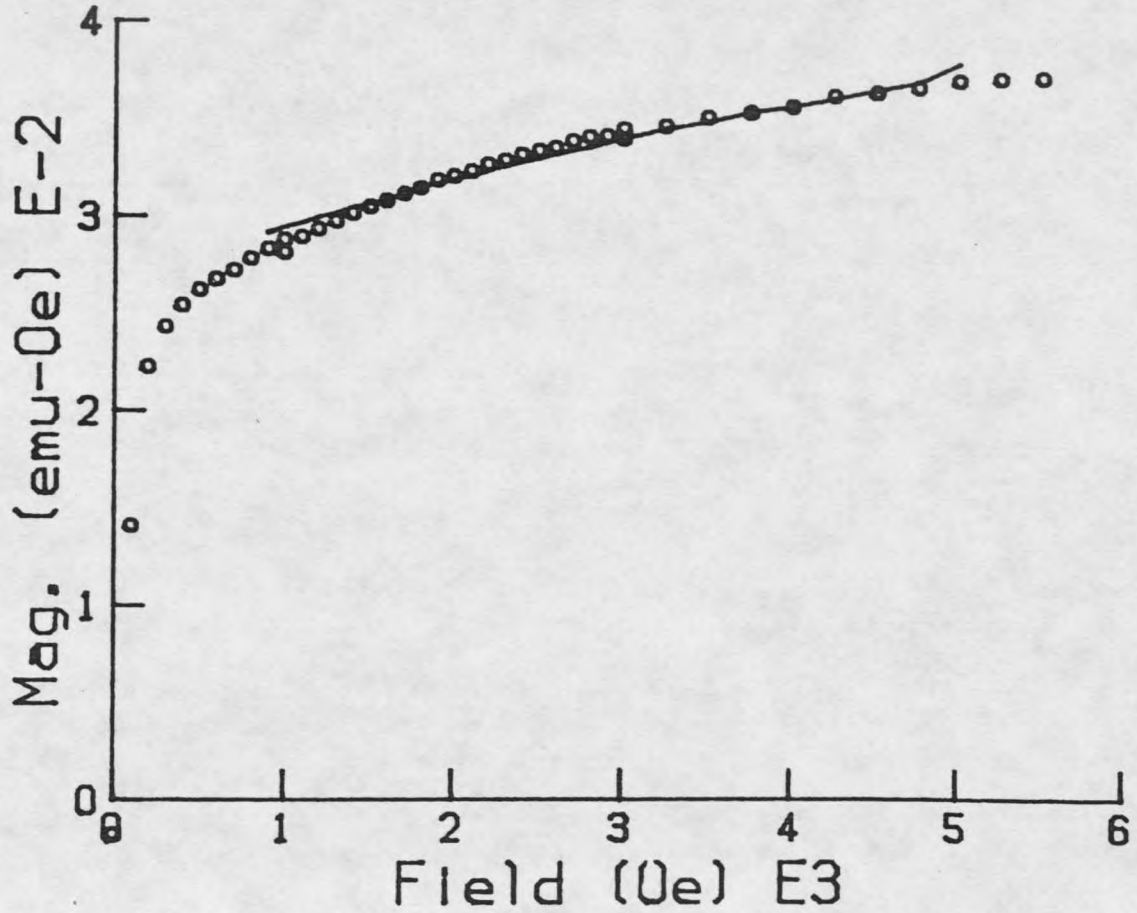

Figure 24. Magnetization versus field fit at T = 3.87 K. Field applied parallel to the z-axis. The line represents the fit to the magnetization curve

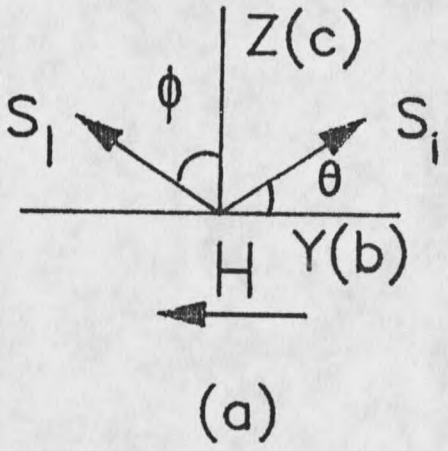

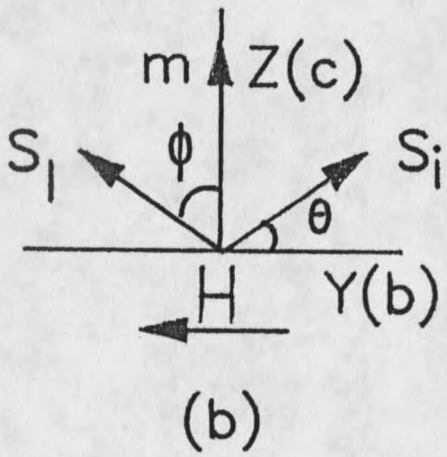

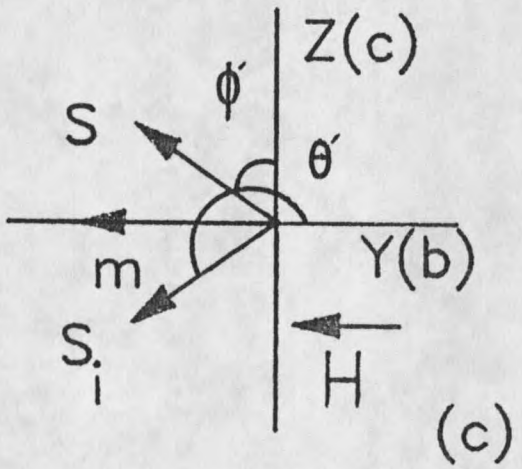

Figure 25. The vector m show the orientation of the resultant magnetization relative to the applied field

parallel to the applied field, which is the lower energy state for this spin structure, see Figure 25 (c). This anomaly happens at a field of 80 Oe and it is a first order phase transition. We call this field spin-twist field. For Figure 25(a) and 25(b) spin structures, the expression for free energy in the molecular field approximation at 0 K with an applied field along the y-axis can be written as:

$$E/g\mu_B S = H_a\cos^2\Phi + H_a\sin 2_\theta + H_{AF}\cos\Phi\sin\theta - H_{AF}\sin\Phi\cos\theta$$

$$- H_d(\sin 2\Phi + \sin 2\theta) - h\sin\Phi + h\cos\theta \qquad (1)$$

and

$$E'/g\mu_B S = H_a\cos^2\Phi' + H_a\sin 2\theta' + H_{AF}\cos\Phi'\sin\theta' - H_{AF}\sin\Phi'\cos\theta'$$

$$- H_d(\sin 2\Phi' + \sin 2\theta') - h\sin\Phi' + h\cos\theta' . \qquad (2)$$

Since E and E' are functions of θ, Φ and θ',Φ'. They can be minimized by setting

$$dE/d\Phi = 0 , dE/d\theta = 0 , dE'/d\theta' = 0 , dE'/d\Phi' = 0 .$$

This gives

$$-H_a\sin 2\Phi - H_{AF}\cos(\Phi-\theta) - 2H_d\cos 2\Phi - h\cos\Phi = 0 \qquad (3)$$

$$H_a\sin 2\theta + H_{AF}\cos(\Phi-\theta) - 2H_d\cos 2\theta - h\sin\theta = 0 \qquad (4)$$

$$-H_a\sin 2\Phi' - H_{AF}\cos(\Phi'-\theta') - 2H_d\cos 2\Phi' - h\cos\Phi' = 0 \qquad (5)$$

$$H_a\sin 2\theta' + H_{AF}\cos(\Phi'-\theta') - 2H_d\cos 2\theta' - h\sin\theta' = 0 \qquad (6)$$

Furthermore, E and E^{l} are equal at the spin-twist field. By the use of $(2H_{AF} + H_a) = 2150$ Oe, $H_d = 2600$ Oe and the experimental value of the spin-twist field of 80 Oe, Equations (1) through (6) have been solved simultaneously. The resultant values for H_{AF} and H_a are 300±50 Oe and 1550 ± 50 Oe, respectively. Now we can use Equations (5) and (6) to determine the angles θ^{l} and Φ^{l} as a function of field. With θ^{l} and Φ^{l} at our disposal, we can calculate magnetization as a function of applied field. This has been done and the results are presented in Figure 26, where circles represent experimental data and the solid line represents the calculated values. The agreement between the data points and calculated values are good within the experimental error. Figure 27 shows E and E^{l} as a function of the applied field. E and E^{l} have equal energies at about 100 Oe, which is close to the experimental value of 80 Oe.

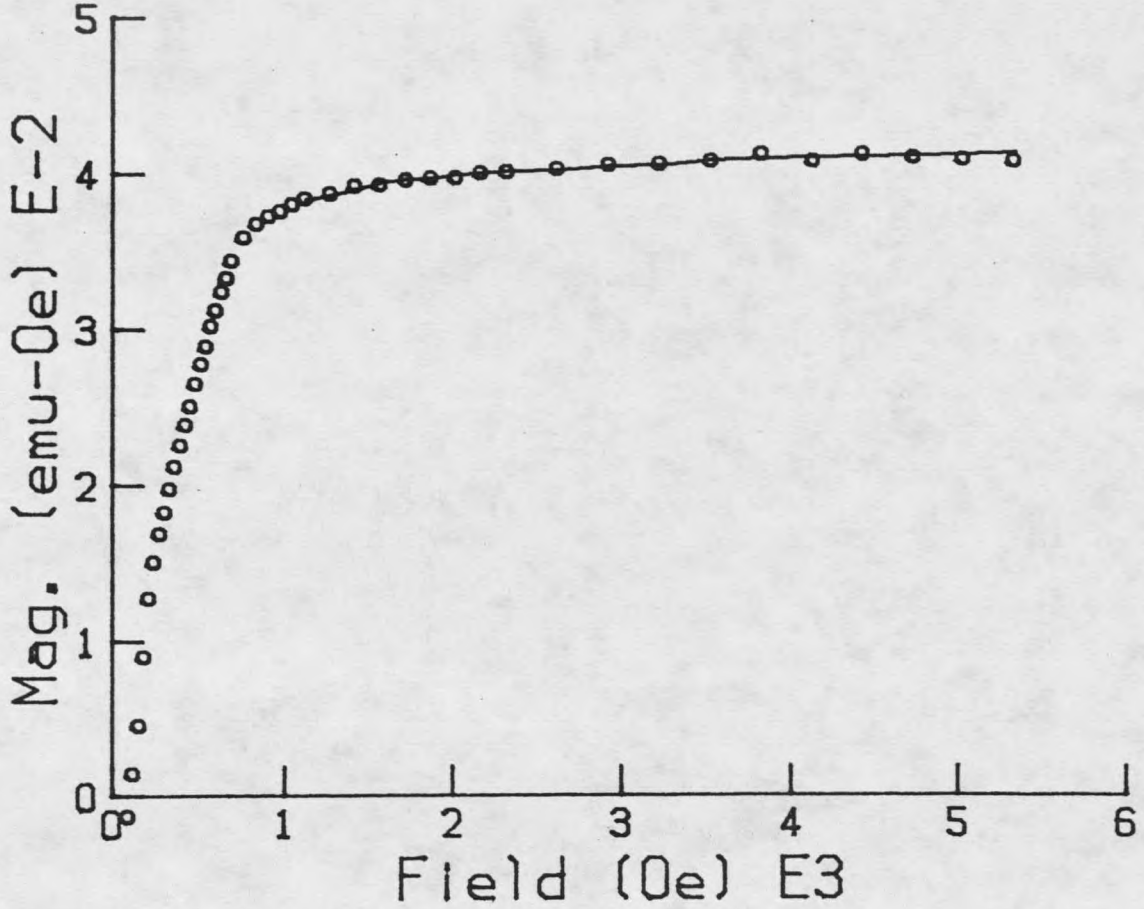

Figure 26. Magnetization versus applied field fit at T = 2.2 K, field applied parallel to the y-axis. The line represents the fit to the magnitization curve

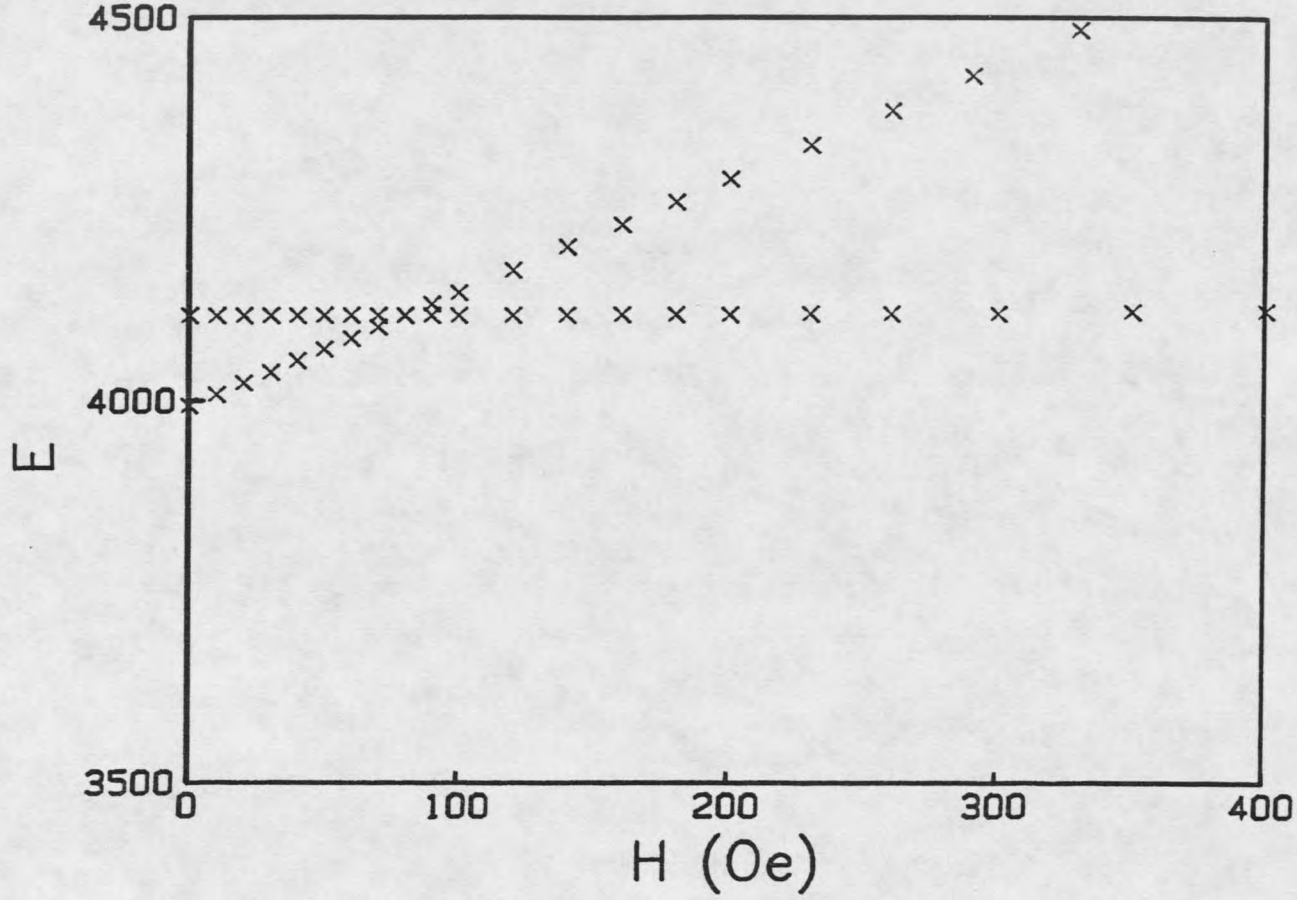

Figure 27. Calculated energy versus applied field. Field is applied along the y-axis

CHAPTER FIVE

MAGNETIC PHASE DIAGRAM

In this chapter, we will use the results of Chapter 2 to discuss the magnetic phase diagram of C2Br. The magnetic phase diagram of $(C_2H_5NH_3)_2CuBr_4$ has been obtained from measurements of susceptibility as a function of field and temperature. Figure 28 shows the H-T diagram along the y-axis. This figure illustrates three distinct phase boundaries. These are: 1) paramagnetic (P) to canted antiferromagnetic (CAF); 2) CAF to spin-twist (ST); and 3) ST to P phase boundaries. Note that the three phase boundaries meet at a bicritical point H = 60 ± 5 Oe and T = 10.74 ± 0.05 K. The temperature dependent susceptibilities, see Figure 12, have been used to construct the second order P to CAF phase boundary. The field dependent magnetization measurements, see Figure 17, indicate a nearly constant value for the CAF to ST transition field. We used these measurements to construct the first order CAF to ST phase boundary. It should be noted that, in constructing the CAF-ST boundary, we simply plotted H and T values at which dM/dH was maximum. Since this was done by observation, an error of ± 10 Oe is expected. The magnetization curves of Figures 31-34 of the appendix were used to construct the second order ST to P phase boundary.

The CAF - ST phase boundary is nearly temperature independent, so we can easily determine the spin-twist field at zero temperature as

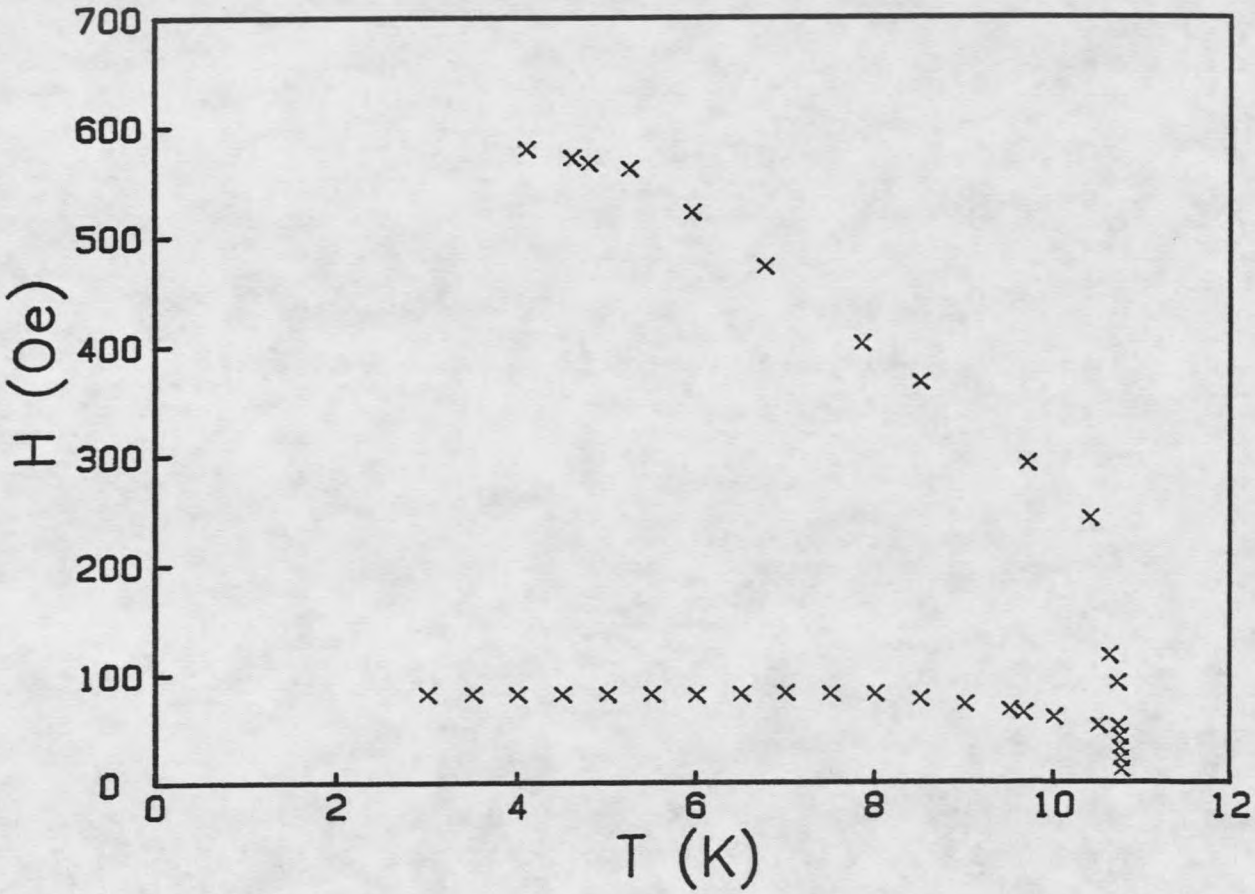

Figure 28. Magnetic phase diagram along the y-axis

$H_{ST}(0)= 80 \pm 5$ Oe. The value for the critical field $H_c(T=0)= 630 \pm 50$ Oe is determined by extrapolating the ST-P phase boundry to zero temperature.

The magnetic phase diagrams along x and z axis are illustrated in figures 29 and 30, respectively. These diagrams were determined by means of two kinds of experiments. These two experiments are magnetization versus field and susceptibility versus temperature. The phase diagram along x axis was obtained from figures 14 and 35 through 38 of the appendix. Similarly H-T diagram along z-axis was constructed from figures 14 and 38 through 40 of the appendix.

The critical fields extrapolated to zero temperature are 650 ± 50 Oe and 130 ± 20 Oe for the magnetic phase diagrams along x and z axes, respectively.

There is a certain anisotropy energy which causes the spins to align along a preferred direction. This anisotropy energy can be expressed in terms of a field H_A. In the case of C_2Br the contributors to the anisotropy field are H_a and H_d. In Chapter Two, we showed by molecular field theory that

$$H_{SF}(0) = [2H_{AF}H_A - H_A^2]^{1/2} \qquad (1)$$

and

$$H_c(0) = 2H_{AF} - H_A \qquad (2)$$

Since C_2Br is a canted antiferromagnet, Equations (1) and (2) cannot be used. However, it is interesting to note the following observation. The

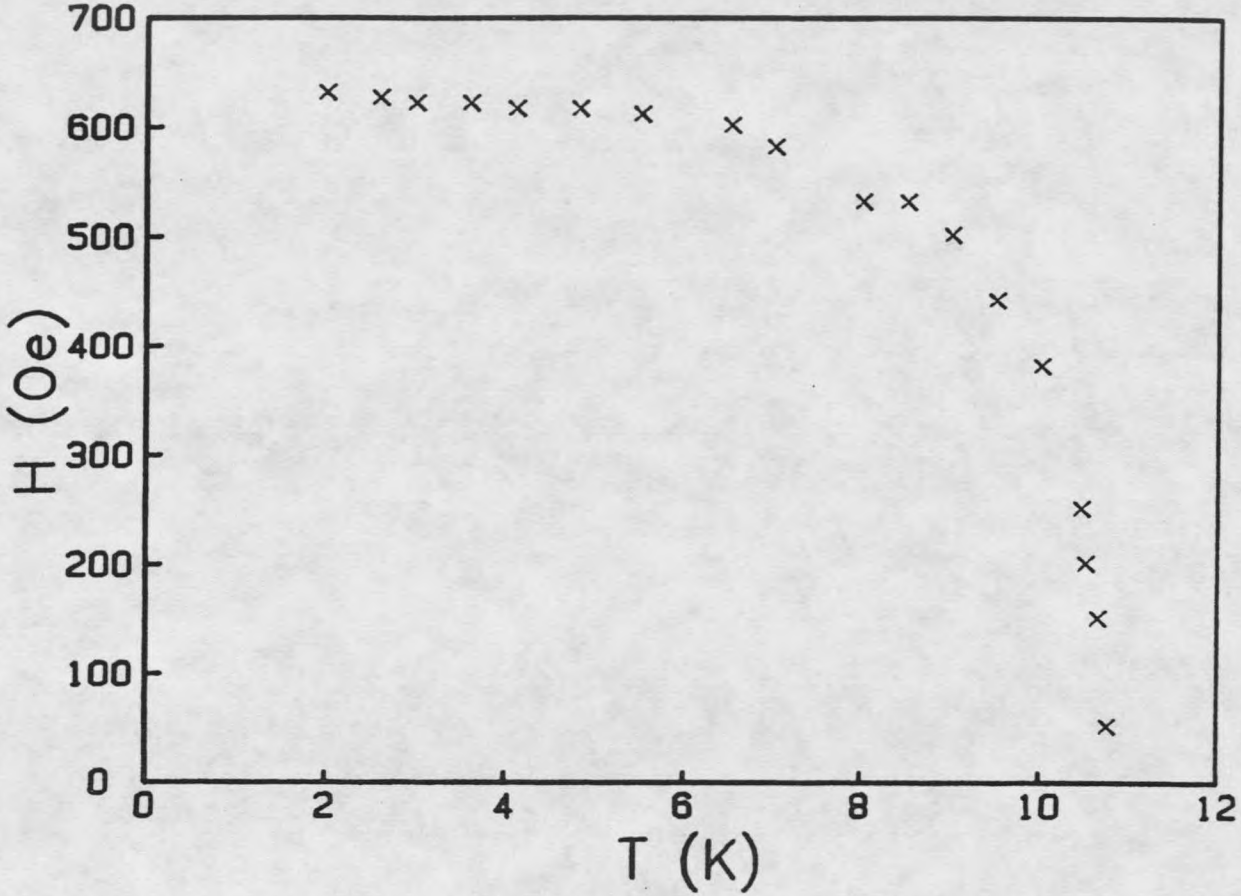

Figure 29. Magnetic phase diagram along the x-axis

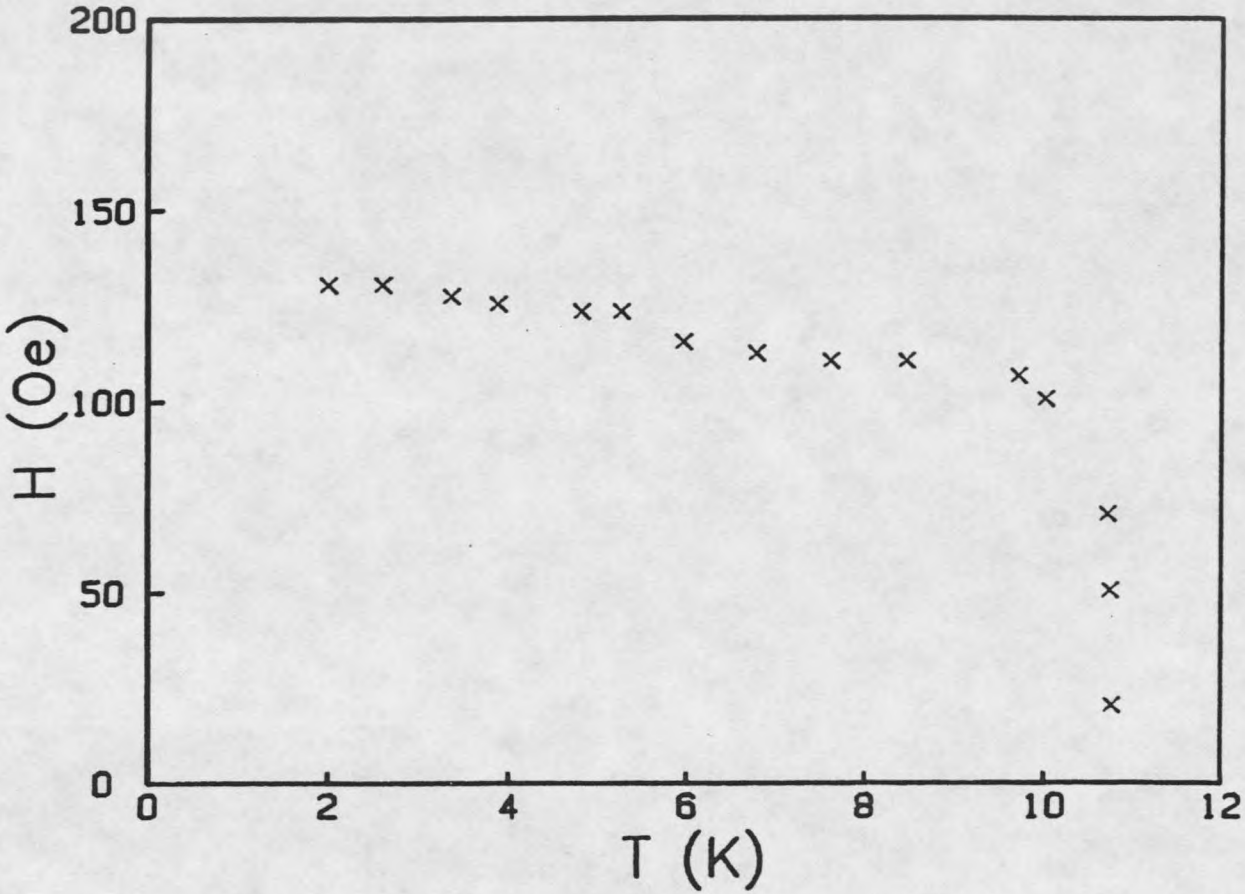

Figure 30. Magnetic phase diagram along the z-axis

magnitude of experimental spin-twist field (H_{ST} = 80 ± 5 Oe) indicates that H_a and H_d are in opposition to each other, therefore we define

$$H_A = H_d \cos\theta - H_a , \qquad (3)$$

where θ is the angle between spin S_i and the z-axis at zero temperature (see Figure 23). For the spin-twist field and the critical field, Equations (1) and (2) become

$$H_{ST}(0) = [2H_{AF}(H_d \cos\theta - H_a) - (H_d \cos\theta - H_a)^2]^{1/2} \qquad (4)$$

and

$$H_c(0) = 2H_{AF} - (H_d \cos\theta - H_a) . \qquad (5)$$

We use Equations (4) and (5) to estimate the values of the antiferromagnetic exchange field, H_{AF}, and the angle θ , using the previously obtained values H_d = 2600 Oe, H_A = 1550 Oe, H_{ST} = 80 Oe, H_c = 650 Oe, and find for the antiferromagnetic exchange field and angle

$$H_{AF} = 320 \text{ Oe.}$$

$$\theta = 53.2 \text{ degrees.}$$

These values agree rather well with H_{AF} = 300 ± 50 Oe obtained in Chapter 4 and the reported value of θ = 49.5 degrees by Yoshio.

CHAPTER SIX

CONCLUSION

The result of this thesis can be formulated as follows:

1. In accordance with the model proposed by Yoshio, it has been shown experimentally that below T_N= 10.78 K C_2Br goes into an antiferromagnetic state which has weak ferromagnetism.
2. The experimental data were fitted to the simple quadratic Heisenberg model and ferromagnetic exchange interaction, J/k=18.5 K; transition temperature, J/kT_c=1.72; Curie constant, C=0.4739 emu-K/mole; and Curie-Weiss temperature, θ=37 K were obtained. The system, at high temperature, showed the behavior expected for a two dimensional Heisenberg ferromagnet.
3. We obtained the magnetic parameters by the mean field calculation to be H_a= 1550 ± 50 Oe, H_d= 2600 ± 50 Oe, and H_{AF}= 300 ± 50 Oe.
4. When an increasing applied field was directed along the z-axis an anomaly was observed at a field of 80 Oe. We called this field spin-twist field. This first order transition is due to sudden reorientation of the ferromagnetic moment, m, in the yz plane.
5. We constructed the magnetic phase diagrams along the x, y, and z-axes. The phase diagram along the y-axis has three distinct phase boundaries. These are: 1) P to CAF; 2) CAF to ST; and, 3) ST to P phase boundaries. Furthermore, we found spin-twist field and critical field follow the following formulas:

$$H_{ST}(0)=[2H_{AF}(H_d\cos\theta-H_a)-(H_d\cos\theta-H_a)^2]^{1/2}$$

and

$$H_c(0)=2H_{AF}-(H_d\cos\theta-H_a).$$

The magnetic phase diagrams along the x and z-axes possess two distinct boundaries. These are: 1) P-CAF; 2) CAF-P boundaries. We found the critical fields extrapolated to zero temperature to be 650 ± 50 Oe and 130 ± 20 Oe for the H-T diagrams along x and z axes, respectively.

6. In Chapter 3, we discussed three possible spin arrangements at zero field for this system. These were: 1) four-sublattice magnet; 2) two-sublattice soft canted antiferromagnet; and 3) covert ferromagnet. Our experimental data confirmed that C_2Br is a two-sublattice soft canted antiferromagnet. However, it is possible that this system is a covert ferromagnet and at low external fields, the competition between the terms in the free energy leads to a tilting of the spins in the yz plane. Hopefully, further investigation on this very interesting magnetic system can bring forward more knowledge about spin arrangement at zero field.

REFERENCES CITED

1. Y. Suzuki, K. Tsuku, Y. Kimisishima, and H. Kubo, J. Phys. Soc. Jpn. 50, 1479 (1981).

2. I. Dzyaloshinsky, J.Phys. Chem. Solids 4,241 (1958).

3. L. J. de Jongh and W. D. V. Amstel, J. De Phys. Coll. C1, Supplement au n 2-3, Tome 32, Fevrier-Mars 1971, c1-880.

4. L. J. de Jongh, Physica 58, 277 (1972).

5. L. J. de Jongh, A. C. Botterman, F. R. Boer, and A. R. Miedema, J. App. Phys. 40, 1363 (1963).

6. J. E. Drumheller, D. Raffaelle, M. Baldwin, Am. J. Phys. 54 1130 (1986).

7. K. E. Emerson, private communication.

8. L. Landenburger, M.S. Thesis, Montana State University, (1987).

9. G. V. Rubenacker, Ph.d.Thesis, Montana State University, (1988).

10. A. S. Borovik-Romanov, Soviet Physics JEPT 12, 18 (1961).

11 R. Suhl, Magnetism I, (Academic Press:New York, 1963).

12. H. Kubo, I. Yahara and K. Hirakawa, J. Phys. Soc. Jpn., 41, 442 (1976).

13. P. Bloembergen, P. J. Berkhout and J. M. Franse, Int. J. Magnetism 4, 219 (1973).

APPENDIX

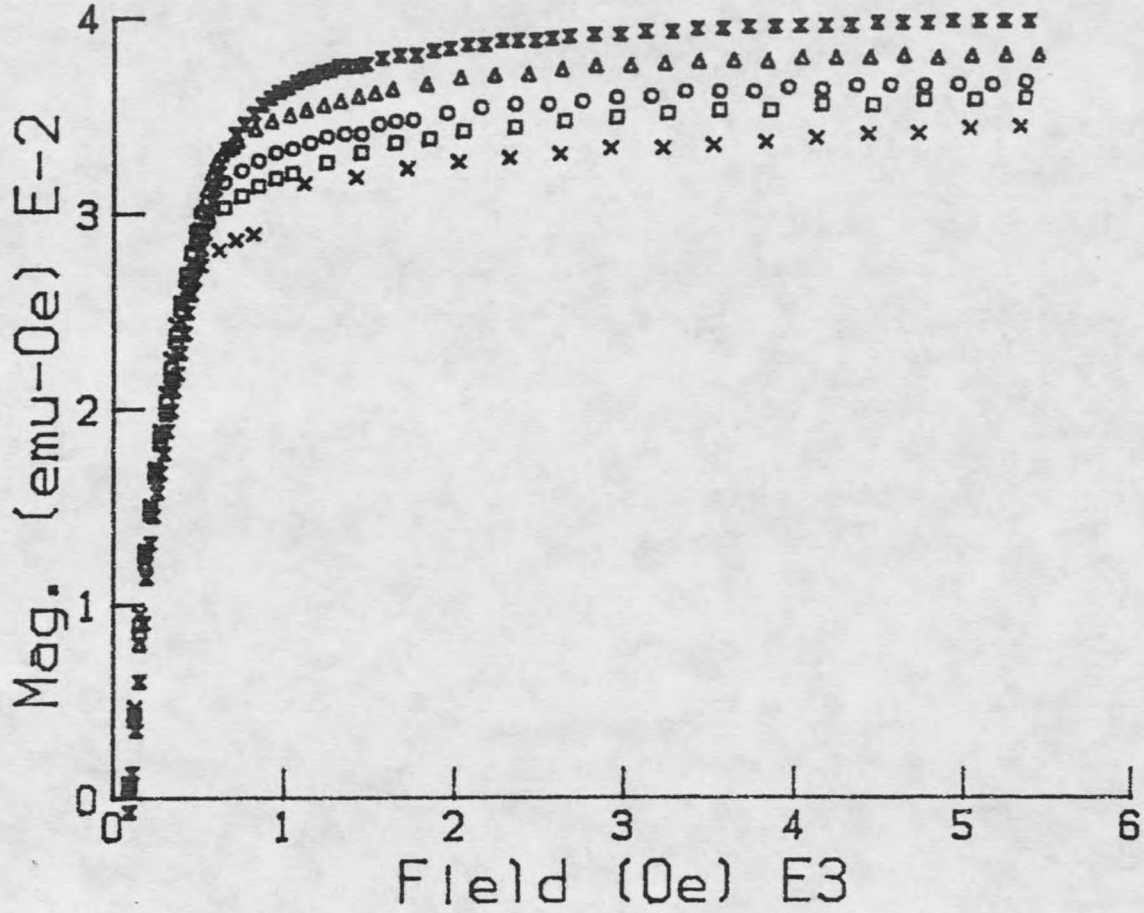

Figure 31. Magnetization versus field at various temperatures, with field applied along the y axis. (dbl.tri., 4K; triangle, 5.5K; circle, 6.5K; square, 7.5K; cross, 8.5K)

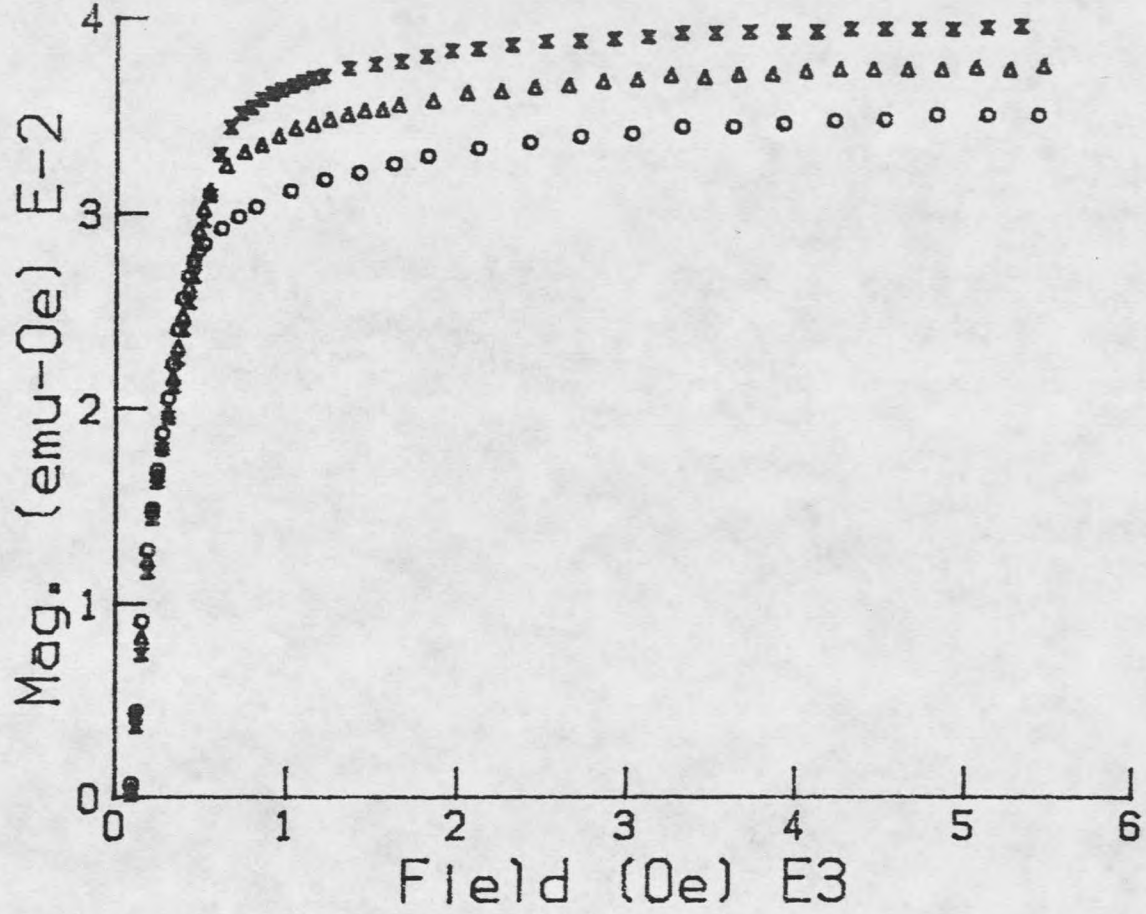

Figure 32. Magnetization versus field at various temperatures, with field applied along the y-axis. (dbl.tri., 4.4K; triangle, 6K; circle, 8K)

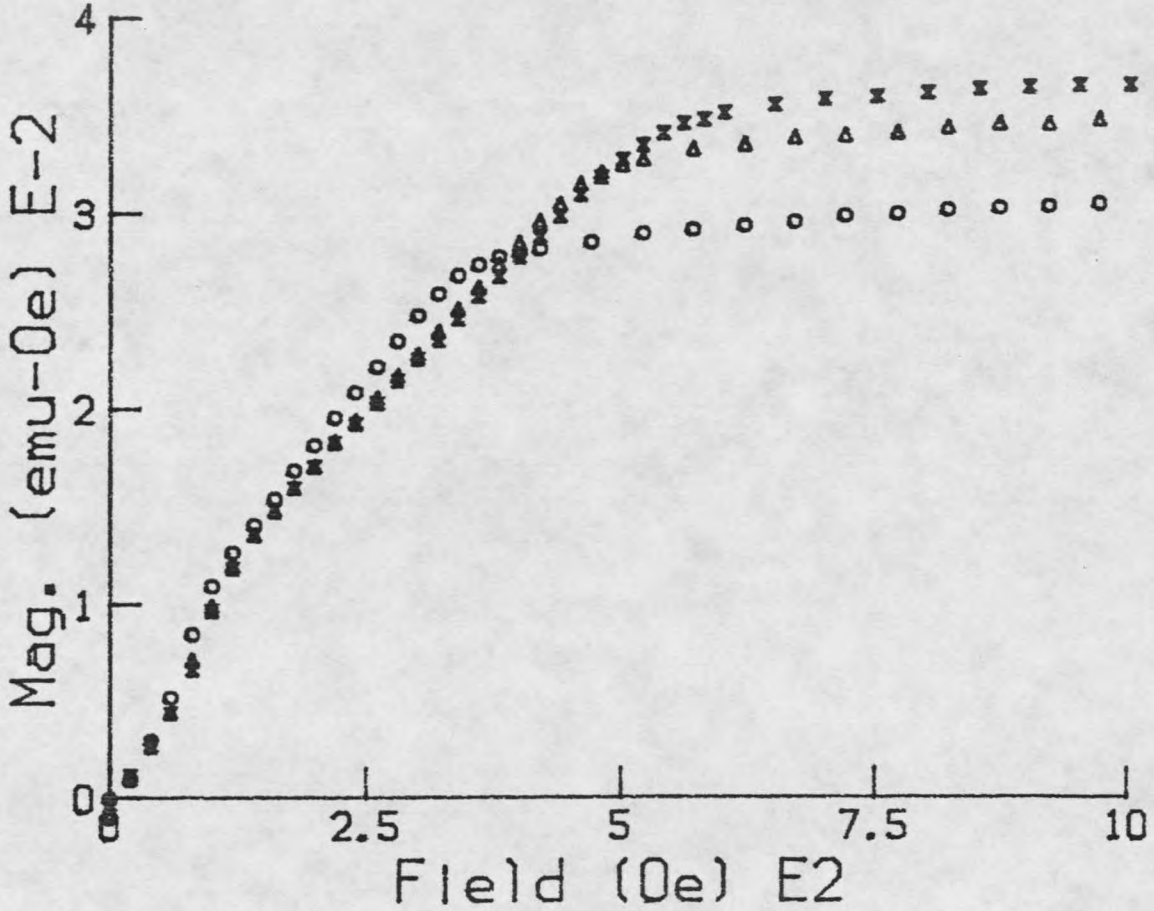

Figure 33. Magnetization versus field at various temperatures, with field applied along the y-axis. (dbl.tri., 4.79K; triangle, 5.95K; circle, 8.5K)

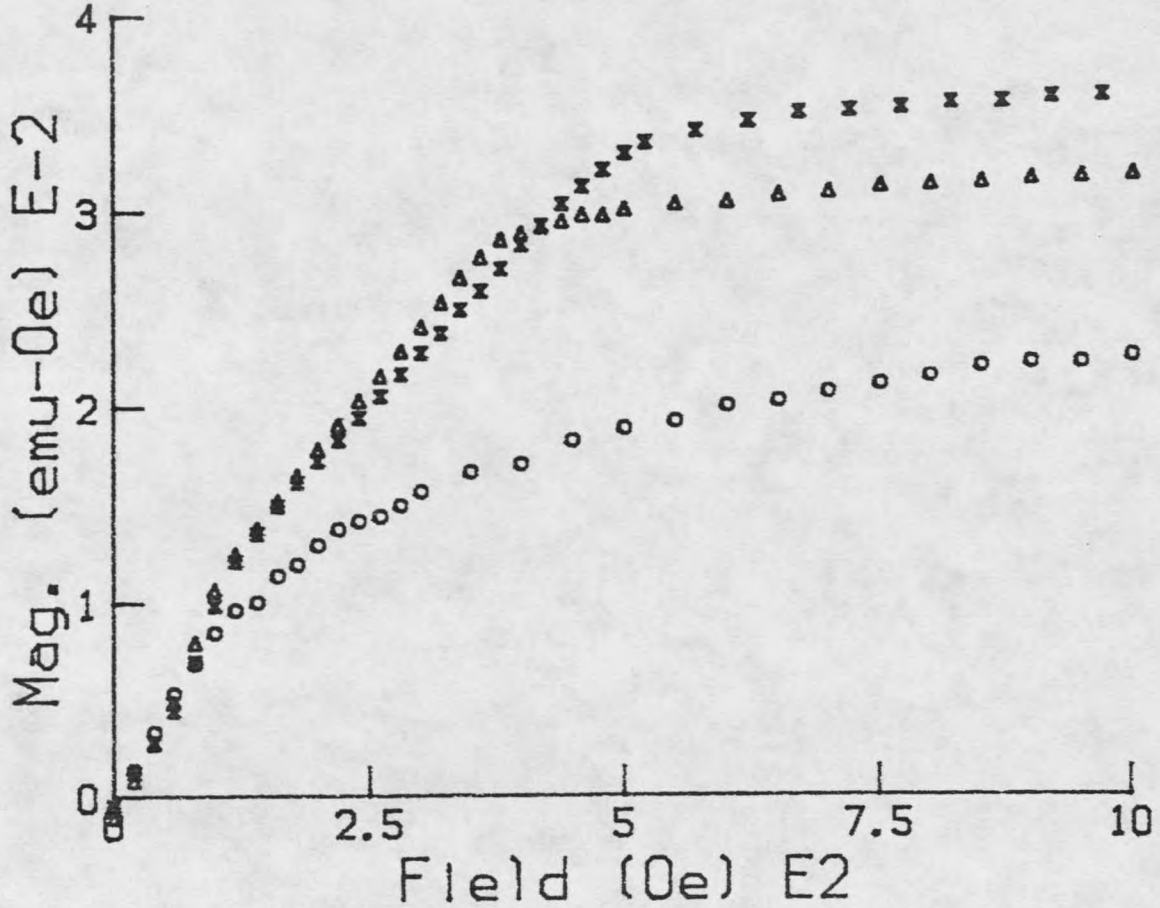

Figure 34. Magnetization versus field at various temperatures, with field applied along the y-axis. (dbl.tri., 5.25K; triangle, 7.85K; circle, 11K)

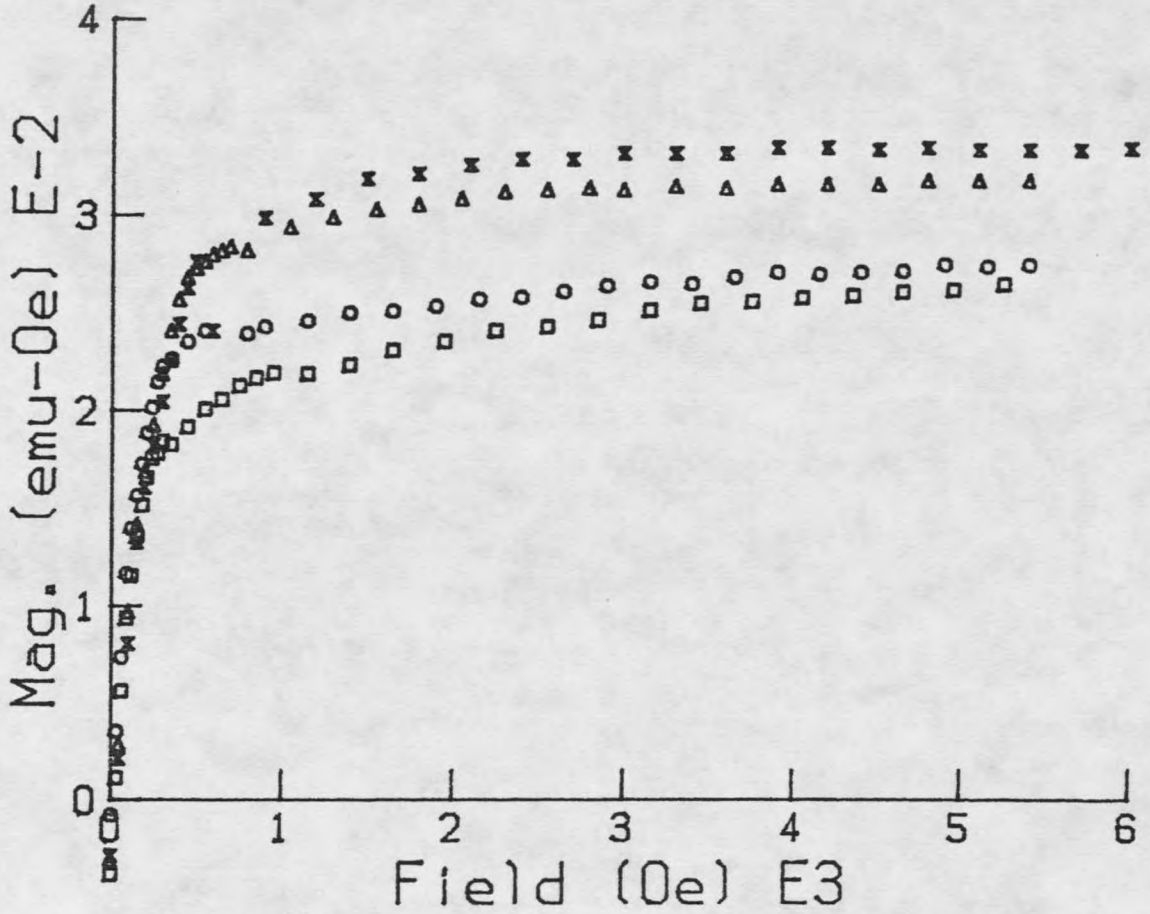

Figure 35. Magnetization versus field at various temperatures, with field applied along the x-axis. (dbl.tri., 4.6K; triangle, 6.5K; circle,9K; square, 10K)

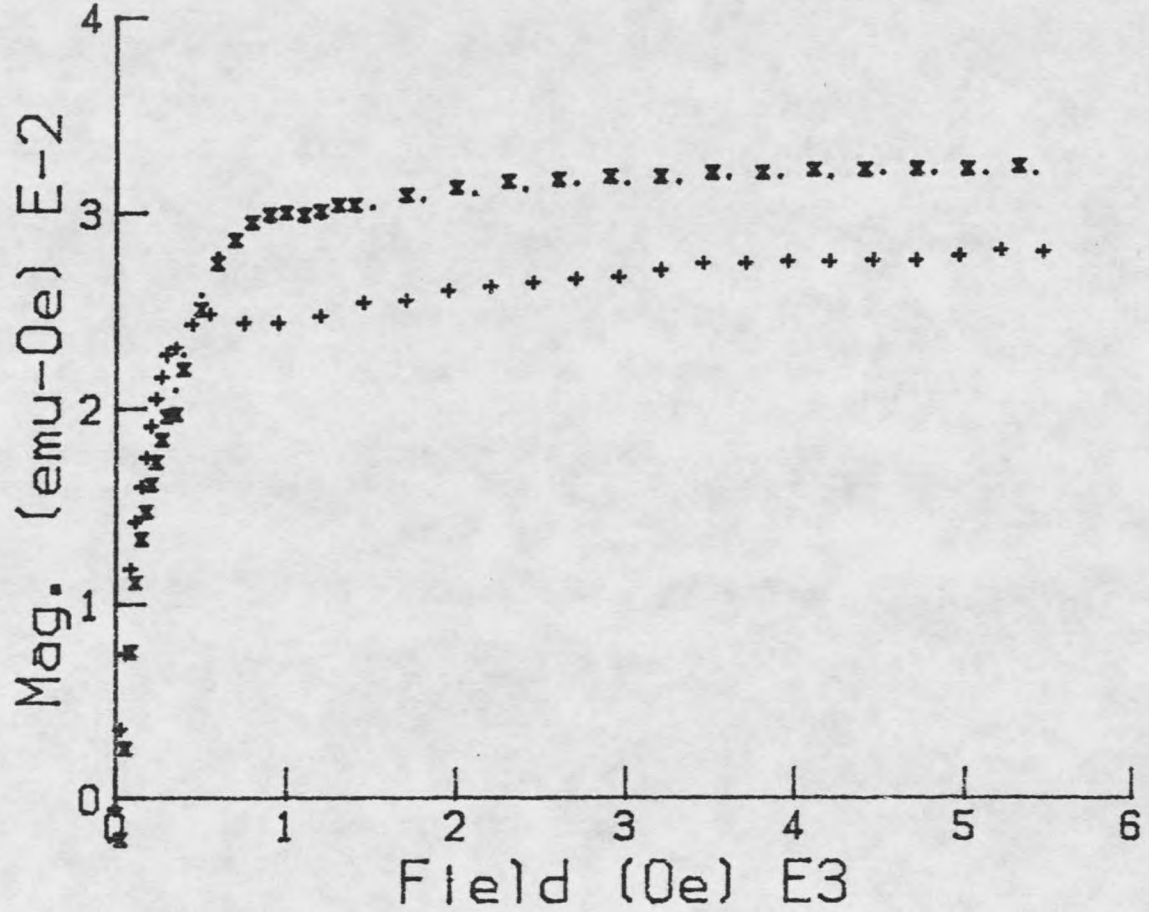

Figure 36. Magnetization versus field at various temperatures, with field applied along the x-axis. (dbl.tri., 2.6K; dot, 3K; plus, 8.5K)

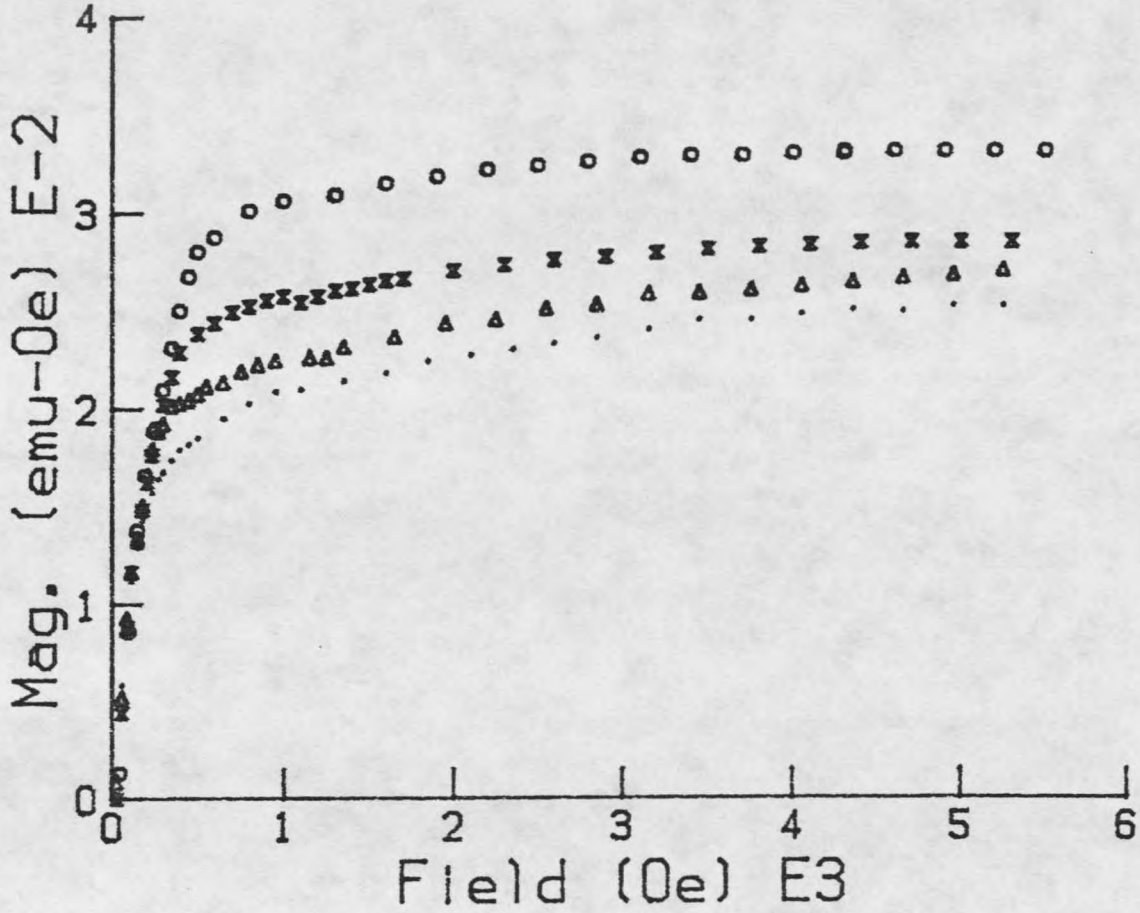

Figure 37. Magnetization versus field at various temperatures, with field applied along the x-axis. (circle, 4.8K; dbl.tri., 7K; triangle, 9.5K; dot, 10.5K)

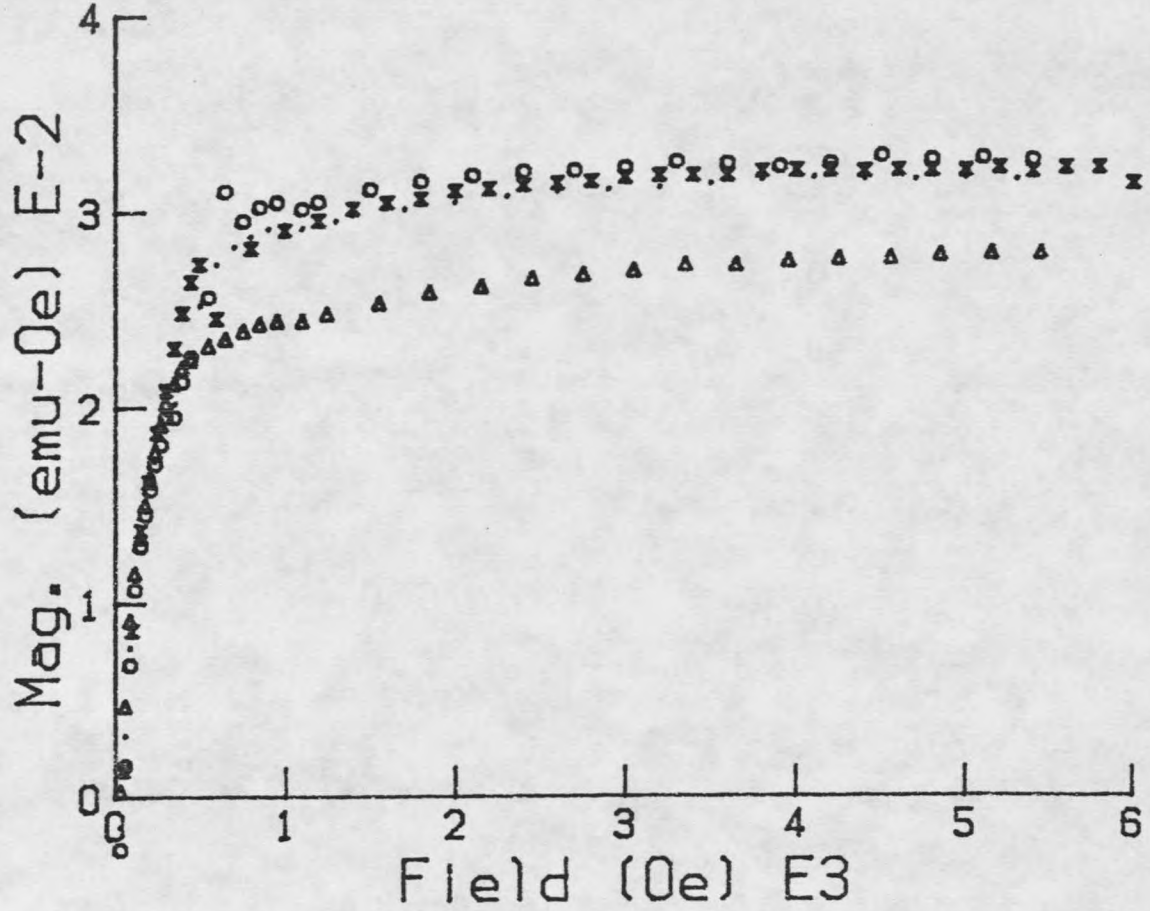

Figure 38. Magnetization versus field at various temperatures, with field applied along the x-axis. (circle, 2K; dot, 3.6K; dbl.tri., 2.6K; triangle, 5.5K)

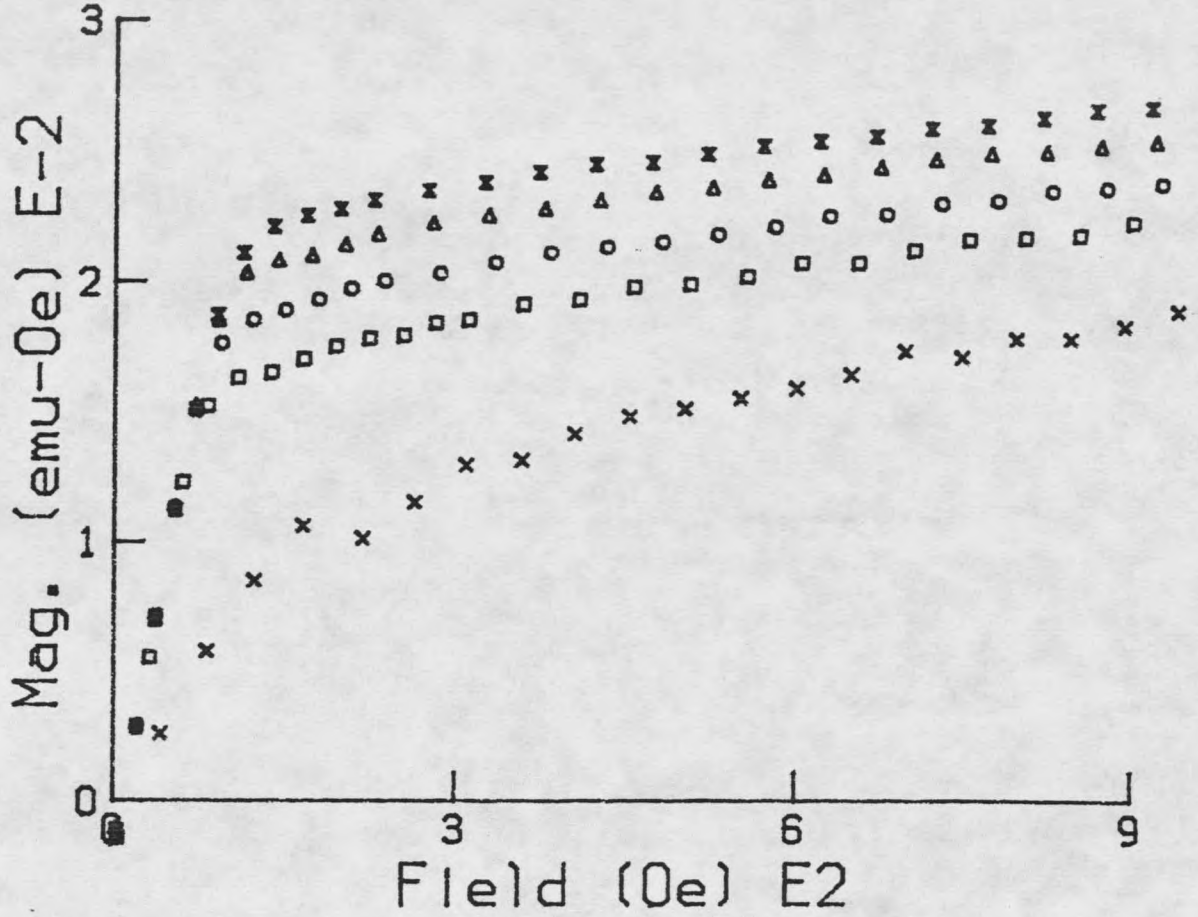

Figure 39. Magnetization versus field at various temperatures, with field applied along the z-axis. (dbl.tri., 5.25K; triangle, 6.77K; circle, 8.45K; square, 9.7K; cross, 11K)

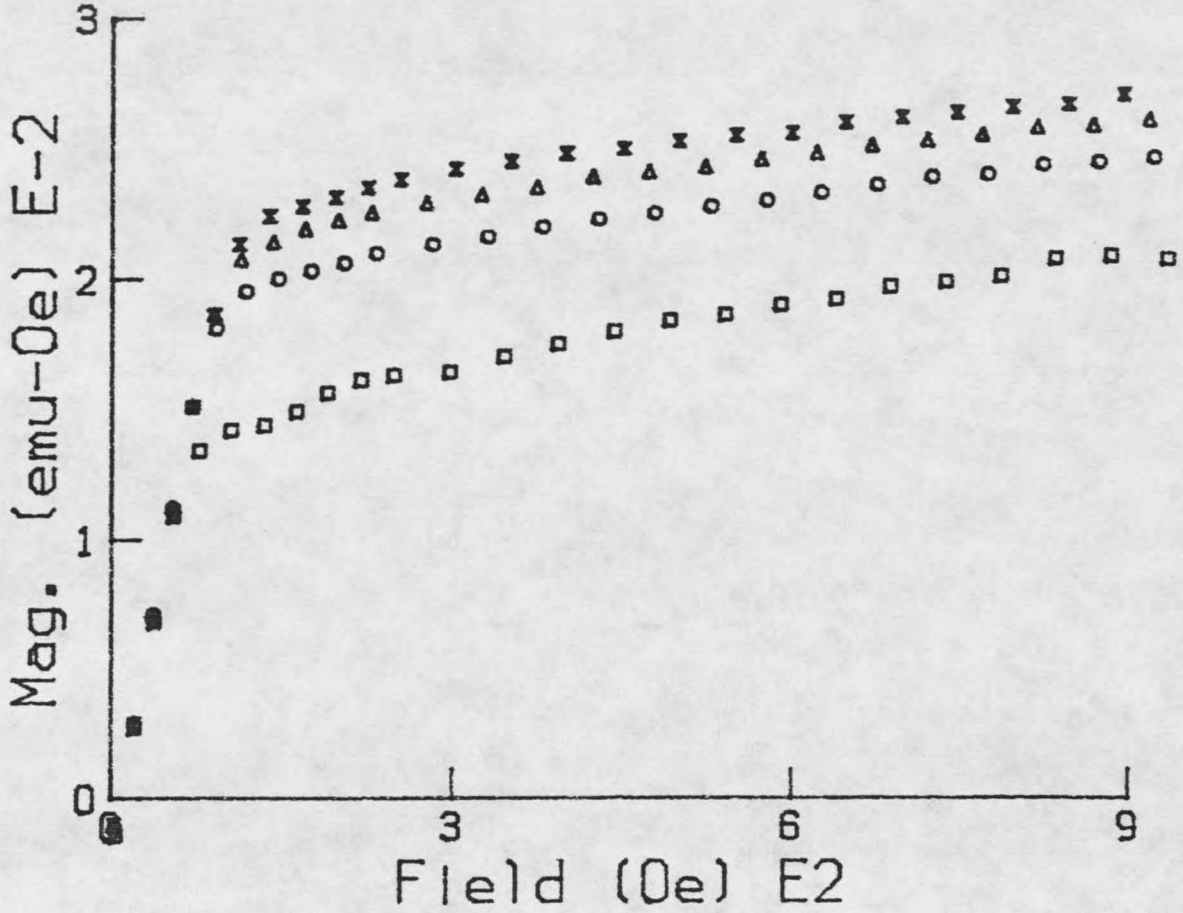

Figure 40. Magnetization versus field at various temperatures, with field applied along the z-axis. (dbl.tri., 4.8K; triangle, 5.95K; circle, 7.6K; square, 10.5K)